An entropy-stable and fully well-balanced scheme for the Euler equations with gravity. II: General equations of state

Victor Michel-Dansac, Andrea Thomann

An entropy-stable and fully well-balanced scheme for the Euler equations with gravity. II: General equations of state

Victor Michel-Dansac[a], Andrea Thomann[a]

[a] *Université de Strasbourg, CNRS, Inria, IRMA, F-67000, Strasbourg, France*

Abstract

The present work concerns the derivation of a fully well-balanced Godunov-type finite volume scheme for the Euler equations with a gravitational potential based on an approximate Riemann solver. It is an extension to general equations of states of the entropy-stable and fully well-balanced scheme for ideal gases recently forwarded in Berthon et al. [9]. When the system is equipped with a convex entropy and associated entropy inequality, it is also entropy-stable and positivity-preserving for all thermodynamic variables. An extension to high order accuracy is presented. Numerical test cases illustrate the performance of the new scheme, using six different equations of state as examples, four analytic and two tabulated ones.

Keywords: Euler equations with gravity, General equations of state, fully well-balanced scheme, Godunov-type scheme, positivity preservation, entropy stability
65M08, 76M12

1. Introduction

The Euler equations with gravity are the core of many models in fluid dynamics, e.g. in astrophysics or meteorology. Therein, the hydrodynamic evolution of atmospheres is often described by the full or barotropic Euler equations. Since these atmospheres are usually a stable system, they are often in an equilibrium configuration, and processes like convection can be viewed as perturbations of the underlying steady state. Depending on the event that is observed, these perturbations can vary by several orders of magnitude. For the numerical resolution of those flows, perturbations whose amplitude is smaller than the background error of the applied numerical scheme are quite challenging to properly approximate, even with high order schemes. In these cases, the mesh resolution has to be refined to reduce the background error and make the perturbations visible in the numerical simulation. This leads to a computational overhead, which could be avoided were the numerical scheme able to resolve the underlying equilibrium state with high accuracy, or even at machine precision.

These are so-called well-balanced schemes, a name which was coined in the pioneering work [13] of Cargo & LeRoux. They were the first to construct a scheme for the Euler equations with gravity source terms capable of preserving exactly a discrete form of a hydrostatic equilibrium. Further, in the work of Bale & LeVeque [34] within the quasi-steady wave-propagation framework, the source term was numerically included in the Riemann problem, a technique extended from shallow-water equations to the Euler equations with an ideal gas law. Since then, a lot of research has been devoted to the development of well-balanced schemes, more particularly in the context of the shallow water equations. For instance, [1, 40, 57, 7, 18, 12] is a non-exhaustive list of contributions to the topic. For the Euler equations, much work has been dedicated to numerically preserving the special class of stationary

hydrostatic atmospheres [30, 23, 35, 4, 56]; see also Käppeli's detailed review [33] for an overview of techniques and concepts.

More recently, so-called moving steady states got more and more attention, first in the context of the shallow water equations [36, 15, 39, 37], but also for general systems [25, 16, 3, 6, 21]. For the Euler equations, strategies that were effective for hydrostatic equilibria are often adapted to achieve well-balanced solutions for some moving equilibria. For example, in [32], a method was developed to preserve a constant, non-zero velocity in a single grid-aligned direction.

Besides the well-balanced property, a key property for robustness is entropy stability. For the Euler equations, on the analytical level, an accompanying inequality, the entropy inequality, can be derived. So-called admissible entropy weak solutions of the Euler equations satisfy this relation, which is important for excluding numerical solutions which are not thermodynamically compatible [45, 46]. To ensure that the numerical solution is the physical admissible entropy solution, the numerical method has to fulfil the discrete analogue of this entropy inequality. Such schemes are then called entropy-stable. Their construction is quite challenging and a lot of work was dedicated to deriving entropy-stable schemes for the homogeneous Euler equations [28, 24, 10, 5, 17, 19], and also entropy-stable well-balanced schemes which preserve hydrostatic equilibria [19, 48]. Recently, an entropy-stable fully well-balanced scheme for the Euler equations was constructed in [9] which preserves both hydrostatic and moving equilibria. It belongs to the family of so-called structure-preserving numerical schemes, i.e., schemes where physical properties of the model are preserved within the discrete numerical solution. Besides fulfilling the entropy inequality, it guarantees the positivity of thermodynamic quantities, namely density, pressure, temperature, etc.

Another feature of the Euler equations is that an additional relation, linking the pressure to the density and the internal energy, is needed to close the system. This relation is called the equation of state (EOS). A standard assumption (made in e.g. [9]) to simplify the numerical resolution is to consider ideal gas law, which is a special case of a general EOS. Such an EOS assumes that the modelled fluid is a gas, whose particles are point-like and do not interact with each other. However, this assumption is quite restrictive and limits the applicability of the numerical scheme. Consequently, for real applications, other EOSs are often considered. In [31], a general EOS was considered when well-balancing barotropic hydrostatic equilibria. This numerical scheme was then extended in [27] to steady adiabatic flows with grid-aligned streamlines. Also, in [52], hydrostatic equilibria with classical van-der-Waals gases and van-der-Waals gases with radiation pressure were considered. However, these are only special examples and their extension to general EOS is, at times, quite technical and challenging.

Therefore, this work is dedicated to the construction of a fully well-balanced scheme for general equations of state, which is also entropy-stable in the region of thermodynamical compatibility, i.e., in regions where the weak solution of the Euler equations fulfills an accompanying entropy inequality. As in the ideal gas case, the positivity of thermodynamical variables follows from the entropy stability and the provable positivity of the density. To our knowledge, this is the first time that the entropy stability was rigorously proven and applied to the case of fully well-balanced schemes for general equations of states. The scheme can be applied on analytically available equations of states or on tabulated ones, which increases its applicability.

The resulting scheme is quite simple to implement, as results from a mere modification of intermediate states in the Riemann solver and source term discretization. Moreover, despite the EOS being potentially nonlinear, we highlight that the scheme itself does not feature any nonlinear iteration, except when computing the EOS itself. As a consequence, we wish to preserve this property when developing a high-order well-balanced extension. In the literature, such extensions usually require solving non-linear systems, see e.g. the non-exhaustive list [14, 55, 11, 25]. To avoid solving additional

non-linear systems, we follow the procedure described in detail in [6] and used e.g. in [38] for the shallow water equations. Note that by adopting a strategy that circumvents non-linear iterative solvers in the high-order extension, the associated computational overhead is avoided.

The paper is organized as follows. The next section is dedicated to the Euler equations with gravity, where the model is detailed, and its equilibrium solutions are derived. This section also contains the definition of the equations of state used in the numerical simulations, namely four with analytical expressions and two tabulated ones. Finally, the accompanying entropy inequality for ideal and general EOSs is also addressed. The numerical scheme is derived in Section 3, which contains the derivation of the approximate Riemann solver. First, we describe the general framework of the Godunov-type finite volume scheme, and the conditions that have to be fulfilled by the associated approximate Riemann solver. Namely, we give a proper definition of important concepts such as consistency, well-balancedness, entropy stability and positivity A detailed derivation of all free parameters in the Riemann solver, together with a summary of the resulting numerical scheme and its properties, concludes the section. Section 4 follows, containing numerical test cases, where the accuracy, well-balanced property and performance of the numerical scheme with respect to the resolution of perturbations is assessed. The results are obtained with the ideal gas law, three cubic EOSs, and two tabulated ones. Finally, Section 5 concludes this work.

2. The Euler equations with gravity

We consider, in a one-dimensional setting, the compressible Euler equations with a gravitational source term. They are governed by

$$\begin{cases} \partial_t \rho + \partial_x(\rho u) = 0, \\ \partial_t(\rho u) + \partial_x(\rho u^2 + p) = -\rho \partial_x \varphi, \\ \partial_t E + \partial_x((E+p)u) = -\rho u \partial_x \varphi. \end{cases} \tag{2.1}$$

Therein $\rho > 0$ denotes the density, $u \in \mathbb{R}$ the velocity and $E > 0$ the total energy density. Moreover, $\varphi : \mathbb{R} \to \mathbb{R}$ is a given time-independent continuous gravitational potential. To close the system, we consider a pressure law $p(\tau, e) : \mathbb{R}^+ \times \mathbb{R}^+ \to \mathbb{R}^+$, given in terms of specific volume $\tau = 1/\rho$ and specific internal energy e, which will be defined by different equations of state (EOSs) detailed later on. Moreover, in accordance with the second law of thermodynamics, we assume the existence of a specific (mathematical) entropy $s(\tau, e) : \mathbb{R}^+ \times \mathbb{R}^+ \to \mathbb{R}$, obeying, for some temperature $T(\tau, e) > 0$, the Gibbs relations

$$\frac{\partial s}{\partial \tau}(\tau, e) = -\frac{p(\tau, e)}{T(\tau, e)} < 0, \qquad \frac{\partial s}{\partial e}(\tau, e) = -\frac{1}{T(\tau, e)} < 0. \tag{2.2}$$

The total energy E is then given by summing the internal and kinetic energies, and we get

$$E = \rho e(\tau, s) + \frac{1}{2}\rho u^2. \tag{2.3}$$

Note that, for arbitrary $\tau > 0$, the function $e \mapsto s(\tau, e)$ is strictly decreasing, according to (2.2). Therefore, it is injective (and even bijective), and we can define the inverse function $e(\tau, s)$, used in (2.3). Other quantities of interest include the specific enthalpy h and the specific total enthalpy H, respectively defined by

$$H = h + \varphi, \quad \text{with} \quad h = \frac{E+p}{\rho}. \tag{2.4}$$

To shorten notation, we write system (2.1) in the following compact form

$$\partial_t W + \partial_x F(W) = S(W),$$

where the state vector W, flux function F and source term S are respectively defined by

$$W = \begin{pmatrix} \rho \\ \rho u \\ E \end{pmatrix}, \quad F(W) = \begin{pmatrix} \rho u \\ \rho u^2 + p \\ u(E+p) \end{pmatrix}, \quad \text{and} \quad S(W) = \begin{pmatrix} 0 \\ -\rho \partial_x \varphi \\ -\rho u \partial_x \varphi \end{pmatrix}.$$

Equipped with this notation, most thermodynamical quantities can be expressed in terms of W (and φ if needed). For instance, the specific total enthalpy H can be seen as a function $H(W, \varphi)$, and the entropy s as a function $s(W)$. In (2.1), we require the density ρ and pressure p to be positive. Thus, the state vector W belongs to the set of admissible states Ω, defined by

$$\Omega = \left\{ W \in \mathbb{R}^3 \ \text{ such that } \ \rho > 0 \text{ and } \ p > 0 \right\}. \tag{2.5}$$

To reflect the influence of the gravitational source term on the wave structure of the Euler equations, we augment system (2.1) by adding the (trivial) equation $\partial_t \varphi = 0$. The resulting system is hyperbolic, with eigenvalues

$$\lambda_\pm = u \pm c, \quad \lambda_u = u, \quad \lambda_0 = 0,$$

where c denotes the speed of sound, given by

$$c = \sqrt{\left(\frac{\partial p(\rho, s)}{\partial \rho} \right)_s},$$

where the subscript s denotes the derivative taken at constant entropy. This wave structure is represented in the left panel of Figure 1. Note that, compared to the homogeneous system, which is obtained by setting the gravitational source terms in (2.1) to zero, there is a zero eigenvalue associated to the gravitational potential. This leads to a non-ordered wave structure, since $\lambda_\pm$ and λ_u can be positive or negative, depending on the flow. This has a direct consequence on the construction of the Riemann solver, see e.g. [19] where a relaxation model is developed to circumvent the appearance of a zero wave, or [53] where six different cases of wave order configurations had to be taken into account.

2.1. Equilibrium solutions

Time-invariant solutions of (2.1) with a non-zero velocity $u \neq 0$, so-called moving equilibria, are governed by the following system

$$\begin{cases} \partial_x(\rho u) = 0, & \text{(2.6a)} \\ \partial_x(\rho u^2 + p) = -\rho\, \partial_x \varphi, & \text{(2.6b)} \\ \partial_x((E+p)u) = -\rho u\, \partial_x \varphi. & \text{(2.6c)} \end{cases}$$

Assuming smooth enough steady solutions fulfilling (2.6), we obtain from (2.6a) a constant momentum $q_0 \coloneqq \rho u \neq 0$. Substituting and dividing by q_0 in (2.6c), we find that

$$\frac{E+p}{\rho} + \varphi =: H_0, \tag{2.7}$$

where H_0 denotes a constant specific total enthalpy.

Substituting φ from (2.7) into (2.6b), we obtain

$$\partial_x\left(\frac{q_0^2}{\rho}+p\right)=\rho\,\partial_x\left(\frac{E+p}{\rho}\right). \tag{2.8}$$

Arguing the definition (2.3) of E, we find

$$\frac{E+p}{\rho}=e+\frac{1}{2}\frac{q_0^2}{\rho^2}+\frac{p}{\rho},$$

and so (2.8) reduces to

$$-\frac{q_0^2}{\rho^2}\partial_x\rho+\partial_x p=\rho\,\partial_x e-\rho\frac{q_0^2}{\rho^3}\partial_x\rho+\partial_x p-\frac{p}{\rho}\partial_x\rho.$$

Eliminating and rearranging terms simplifies the above expression to

$$-\frac{p}{\rho}\partial_x\rho+\rho\partial_x e=0.$$

Rewriting this relation in terms of specific volume τ, we obtain

$$p\partial_x\tau+\partial_x e=0. \tag{2.9}$$

However, according to the expressions (2.2) of the entropy derivatives, note that

$$\partial_x s=\frac{\partial s}{\partial\tau}\partial_x\tau+\frac{\partial s}{\partial e}\partial_x e=-\frac{p}{T}\partial_x\tau-\frac{1}{T}\partial_x e.$$

Plugging (2.9) into the above expression, we obtain

$$\partial_x s=0. \tag{2.10}$$

Hence, smooth moving steady solutions for a general equation of state, with $u\neq 0$, are necessarily isentropic and are characterized by the constant triplet (q_0,H_0,s_0) given by

$$\rho u=:q_0,\qquad \frac{E+p}{\rho}+\varphi=:H_0,\qquad s=:s_0, \tag{2.11}$$

where s_0 is a constant specific entropy. In practice, starting from a given triplet (q_0,H_0,s_0) and gravitational potential φ, the steady solution in state variables W is obtained by solving the nonlinear system (2.11) with Newton's method.

A special case is given by time-invariant solutions of (2.1) with zero velocity $u=0$, the so-called hydrostatic equilibria. They fulfil the ordinary differential equation

$$\partial_x p=-\rho\partial_x\varphi. \tag{2.12}$$

Since this problem is ill-posed, additional assumptions about the dependence between pressure and density are required. Intensively studied examples are so-called isothermal or isentropic hydrostatic equilibria with constant temperature or constant entropy, respectively. The reader is referred to the review [33] for a non-exhaustive list of numerical methods achieving well-balancing of hydrostatic equilibria using different numerical techniques. In our case, taking the limit as $u\to 0$ in (2.11) yields the isentropic hydrostatic equilibrium.

2.2. Equation of state

In this work, we will examine various equations of state (EOS), including both analytical expressions and tabulated forms.

First, we will consider a general cubic EOS, with the analytical form

$$p(\tau, T) = \frac{RT}{\tau - b} - \frac{a(T)}{(\tau - br_1)(\tau - br_2)}, \tag{2.13a}$$

$$e(\tau, T) = c_v(\tau, T)T + \frac{a(T) - Ta'(T)}{b}\mathfrak{u}(\tau), \tag{2.13b}$$

where R denotes the gas constant, b the covolume, $r_1, r_2 \in \mathbb{R}$ are parameters, and $\mathfrak{u}(\tau)$ is a function specific to each EOS. The function $a(T)$ defines an attraction term, and c_v is the heat capacity at constant volume. It depends on the temperature and the specific volume, as follows

$$c_v(\tau, T) = c_v^0 - \frac{Ta''(T)}{b}\mathfrak{u}(\tau), \tag{2.14}$$

where c_v^0 is a constant. The gas constant R is connected to the ratio of specific heats γ by $R = (\gamma - 1)c_v$. Depending on the definition of the free parameters and functions, one obtains different known equations of state, such as the ideal gas law, van-der-Waals (`vdW`) EOS [50, 49], Redlich-Kwong (`R-K`) EOS [42] or the Peng-Robinson (`P-R`) EOS [41]. The details of the free parameters and functions are given in Table 1. Moreover, the corresponding (mathematical) entropy definition reads

$$s(\tau, T) = -\left(s_0 - \frac{a'(T)}{b}\mathfrak{u}(\tau) + R\log(\tau - b) + c_v^0 \log(T)\right). \tag{2.15}$$

Note that, in the numerical scheme, the entropy is required to be given in terms of τ and e. It can be recovered analytically using (2.15) and the temperature formulas given in Table 2. However, $e(\tau, s)$ is also required by the numerical scheme. Unfortunately, recovering the internal energy in terms of τ and s involves solving a nonlinear equation, which is done numerically by employing Newton's method (except in the `ideal` and `vdW` cases, where a closed form is available).

EOS	r_1	r_2	$a(T)$	$\mathfrak{u}(\tau)$
`ideal`	0	0	0	0
`vdW`	0	0	a_0	$-\dfrac{b}{\tau}$
`R-K`	0	-1	$\dfrac{a_0}{\sqrt{T}}$	$\log\left(\dfrac{\tau}{\tau + b}\right)$
`P-R`	$-1 - \sqrt{2}$	$-1 + \sqrt{2}$	$a_0\left(1 + \kappa\left(1 - \sqrt{T/T_0}\right)\right)^2$	$\dfrac{1}{r_1 - r_2}\log\left(\dfrac{\tau - br_1}{\tau - br_2}\right)$

Table 1: Parameters and defining functions for some cubic EOS, in particular the ideal gas (`ideal`), van-der-Waals (`vdW`), Redlich-Kwong (`R-K`) and Peng-Robinson (`P-R`) EOS. Therein, a_0, κ, c_v^0 and b denote constants which will be specified when setting up the numerical test cases.

Further, we will consider two tabulated EOS from the `CoolProp` library [2], which contains the thermodynamic description of pure and pseudo-pure fluids and mixtures. As examples in the numerical experiments, we choose the IAPWS-95 formulation for water [54], as well as the EOS for methane [44], both included in the `CoolProp` library.

`ideal`	$T(\tau, e)$	$=$	$\dfrac{e}{c_v^0}$
`vdW`	$T(\tau, e)$	$=$	$\dfrac{e - a_0 U(\tau)}{c_v^0}$
`R-K`	$T(\tau, e)$	$=$	$\dfrac{\left(\Xi(\tau, e) + \sqrt[3]{4}e\right)^2}{3\sqrt[3]{4}\, c_v^0\, \Xi(\tau, e)}$, with $\Xi(\tau, e) = \left(\sqrt{27\xi(\tau)^2 c_v^0 - 4e^3} - \xi(\tau)\sqrt{27 c_v^0}\right)^{\frac{2}{3}}$ where $\xi(\tau) = \dfrac{3}{2} a_0 U(\tau)$
`P-R`	$T(\tau, e)$	$=$	$\dfrac{1}{4T_0 (c_v^0)^2}\left(\sqrt{\xi(\tau)^2\kappa^2 + 4T_0 c_v^0\Big((\kappa+1)\xi(\tau) + e\Big)} - \xi(\tau)\,\kappa\right)^2$, with $\xi(\tau) = a_0(\kappa+1)U(\tau)$

Table 2: Temperatures in terms of τ and e for some cubic EOS: cases of the ideal gas (`ideal`), van-der-Waals (`vdW`), Redlich-Kwong (`R-K`) and Peng-Robinson (`P-R`) EOS.

2.3. Entropy inequality

Let us assume that system (2.1) is equipped with a *convex* entropy function $U(W)$ and an entropy flux $G(W)$, which are related by

$$\nabla_W U(W)^\intercal \nabla_W F(W) = \nabla_W G(W)^\intercal. \tag{2.16}$$

After [46, 19], for an ideal gas, the mapping $W \mapsto -\rho\eta(s(W)) =: U(W)$ is convex as soon as η is any smooth function satisfying

$$\eta'(s) \geq 0 \quad \text{and} \quad \gamma\eta''(s) + \eta'(s) \geq 0.$$

Note that this corresponds to the so-called mathematical entropy. Defining $G(W) := \rho\eta(s)u$, the pair $(U(W), G(W))$ forms an entropy-entropy flux pair. Therefore, admissible entropy weak solutions to system (2.1) under the ideal gas law satisfy the entropy inequality (in the sense of distributions)

$$\partial_t(\rho\eta(s)) + \partial_x(\rho\eta(s)u) \leq 0. \tag{2.17}$$

After [46, 20], the entropy stability of (2.1) for an ideal gas is ensured by merely adopting entropies defined by smooth convex functions η of the state variables such that

$$\eta'(s) \geq 0 \quad \text{and} \quad \eta''(s) \geq 0. \tag{2.18}$$

For a general equation of state, the above definition of the entropy-entropy flux pair might not hold any longer.

Therefore, within this work, we restrict ourselves to thermodynamically compatible materials, i.e., materials in a state for which a convex entropy exists and an accompanying entropy inequality (2.17) can be stated. This assumption of course puts a constraint on the admissibility of the state vector W,

see Appendix A, such that the condition (2.18) holds. We thus define the set of thermodynamically compatible states as

$$\Omega^{\text{tc}} = \{W \in \Omega \text{ such that } (\rho\eta(s), \rho\eta(s)u) \text{ is an entropy-entropy flux pair for (2.1)}\}.$$

To extend the region of thermodynamic compatibility, procedures such as the one explained in [29] can be used to modify the EOS and recover the convexity.

Note that the physical entropy is easily recovered by taking the opposite sign in the entropy definition (2.15). Consistently taking either the mathematical or physical entropy does not impact the derivation of the numerical scheme in the next section.

In the following, the objective is to approximate the system (2.1) with an arbitrary EOS. To that end, we derive a Godunov-type finite volume (FV) scheme based on an approximate Riemann solver (A-RS), which is able to preserve moving equilibria up to machine precision, generates admissible solutions in the sense of (2.5), and fulfills all entropy inequalities (2.17) with (2.18) for states in Ω^{tc}.

3. The numerical scheme

We begin with a brief overview of the principle behind Godunov-type finite volume (FV) schemes, relying on approximate Riemann solvers. As is standard in the finite volume framework, we divide the computational domain $I \subset \mathbb{R}$ into non-overlapping sub-cells $C_i = (x_{i-\frac{1}{2}}, x_{i+\frac{1}{2}})$ with center x_i. Then at a given time t^n, the volume average of the solution on cell C_i is defined as

$$W_i^n = \frac{1}{\Delta x} \int_{x_{i-\frac{1}{2}}}^{x_{i+\frac{1}{2}}} W(x, t^n) dx. \tag{3.1}$$

The time is discretized with varying time steps Δt, which, for stability purposes, must follow a CFL (Courant-Friedrichs-Lewy) condition, see [28], relating Δt to Δx and the current flow properties. Then, the new time step is given by $t^{n+1} = t^n + \Delta t$.

In the next section, we develop an approximate Riemann solver (A-RS) for a general EOS, as done in [9] for the ideal gas case.

3.1. The approximate Riemann solver

In the following, we define an A-RS, denoted by $\widetilde{W}$, whose role it is to approximate the solution of the Riemann problems occurring at each cell interface $x_{i+1/2}$ between cells C_i and C_{i+1}. Since this solution is self-similar, the A-RS depends on the variable x/t, and on the two states W_i^n and W_{i+1}^n located on the left and right sides of the interface, respectively. That is to say, the approximate Riemann solution at interface $x_{i+1/2}$ is given by $\widetilde{W}((x - x_{i+1/2})/t; W_i^n, W_{i+1}^n)$.

In this work, we choose an approximate Riemann solution consisting of two intermediate states, as shown in the right panel of Figure 1. Its expression, for given left and right states W_L and W_R, is as follows:

$$\widetilde{W}\left(\frac{x}{t}; W_L, W_R\right) = \begin{cases} W_L & \text{if } x < -\lambda t, \\ W_L^* & \text{if } -\lambda t < x < 0, \\ W_R^* & \text{if } 0 < x < \lambda t, \\ W_R & \text{if } x > \lambda t, \end{cases} \tag{3.2}$$

where the components of the vectors W_L^* and W_R^* read

$$W_L^* = \begin{pmatrix} \rho_L^* \\ q_L^* \\ E_L^* \end{pmatrix} \qquad \text{and} \qquad W_R^* = \begin{pmatrix} \rho_R^* \\ q_R^* \\ E_R^* \end{pmatrix}. \tag{3.3}$$

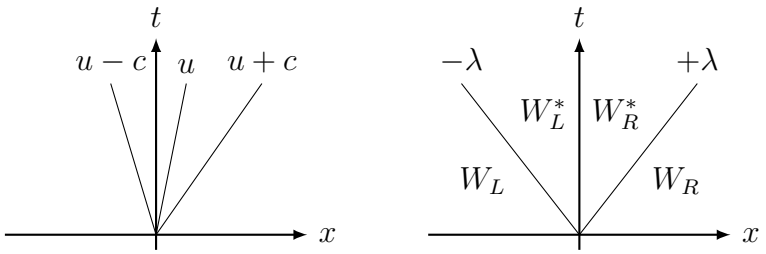

Figure 1: Left panel: One possible wave configuration, with $u > 0$, of the Euler equations with gravity (2.1). Right panel: Wave structure of the approximate Riemann solver.

In the A-RS given by (3.2), the approximate wave speed λ is chosen such that the acoustic waves are included within the A-RS wave fan, i.e., $\lambda \geq |u| + c \geq |\lambda_\pm|$. In this work, we impose symmetry on the waves defining the A-RS around $\lambda_0 = 0$, although this is a simplifying assumption. In principle, two different values of λ could be chosen to capture the asymmetric wave structure of the Euler equations with respect to λ_0, provided that the acoustic waves $\lambda_\pm$ remain within the A-RS. In practice, we set

$$\lambda = \Lambda \max\Big(|u_L| + c(W_L), |u_R| + c(W_R)\Big), \tag{3.4}$$

which indeed satisfies $\lambda \geq |\lambda_\pm|$. The parameter $\Lambda \geq 1$ is merely used to scale the wave speeds, and will be given in the numerical experiments.

Equipped with λ, we can also define a restriction on the time step Δt. Indeed, to ensure the stability of the numerical scheme, the time step must satisfy

$$\Delta t \leq \frac{1}{2}\frac{\Delta x}{\max_i \lambda_{i+\frac{1}{2}}}, \tag{3.5}$$

where $\lambda_{i+\frac{1}{2}}$ is the approximate wave speed at the interface $x_{i+\frac{1}{2}}$, computed by applying (3.4) to the states W_i^n and W_{i+1}^n.

At this level, we have introduced six unknown quantities in (3.3), namely the density, momentum and energy of the intermediate states W_L^* and W_R^*. The remainder of this section is devoted to deriving these unknowns to achieve several crucial properties: the first one, consistency, is the object of the next section.

3.2. Consistency conditions

In this section, we revisit conditions on the intermediate states W_L^* and W_R^* to ensure the consistency of the FV scheme with the solution of the Euler system. These conditions are classical, see [28], and were derived in detail in [9]. Nevertheless, we recall the main steps of their derivation here.

Based on the consistency condition for an A-RS from [28], according to [37], intermediate states must satisfy the following relations

$$\begin{cases} \rho_L^* + \rho_R^* = 2\rho_{\text{HLL}}, \\ q_L^* + q_R^* = 2q_{\text{HLL}} + \dfrac{1}{\lambda\Delta t}\displaystyle\int_{-\Delta x/2}^{\Delta x/2}\int_0^{\Delta t} (-\rho\partial_x\varphi)_{\mathcal{R}}\left(\frac{x}{t}; W_L, W_R\right) dtdx, \\ E_L^* + E_R^* = 2E_{\text{HLL}} + \dfrac{1}{\lambda\Delta t}\displaystyle\int_{-\Delta x/2}^{\Delta x/2}\int_0^{\Delta t} (-q\partial_x\varphi)_{\mathcal{R}}\left(\frac{x}{t}; W_L, W_R\right) dtdx, \end{cases} \tag{3.6}$$

where $(-\rho\partial_x\varphi)_{\mathcal{R}}$ and $(-q\partial_x\varphi)_{\mathcal{R}}$ respectively represent the second and third components of $S(W_{\mathcal{R}})$. This formulation connects the intermediate states of the A-RS with the intermediate state W_{HLL} of the HLL Riemann solver from Harten, Lax and van Leer [28]. It is defined by

$$W_{\text{HLL}} = \begin{pmatrix} \rho_{\text{HLL}} \\ q_{\text{HLL}} \\ E_{\text{HLL}} \end{pmatrix} = \frac{W_L + W_R}{2} - \frac{F(W_R) - F(W_L)}{2\lambda}. \tag{3.7}$$

Moreover, since the entropy plays an important role in the definition of moving equilibria and thus in a fully-well-balanced scheme, we also define the following quantities

$$(\rho s)_{\text{HLL}} = \frac{1}{2}\big(\rho_L s_L + \rho_R s_R\big) - \frac{1}{2\lambda}\big(\rho_R s_R u_R - \rho_L s_L u_L\big), \tag{3.8}$$

$$\big(\rho\eta(s)\big)_{\text{HLL}} = \frac{1}{2}\big(\rho_L \eta(s_L) + \rho_R \eta(s_R)\big) - \frac{1}{2\lambda}\big(\rho_R \eta(s_R) u_R - \rho_L \eta(s_L) u_L\big). \tag{3.9}$$

Therein, we have set $s_L = s(W_L)$ and $s_R = s(W_R)$.

Next, we introduce two new approximate quantities S^q and S^E, approximating the cell averages of the source terms:

$$\begin{aligned} S^q &\approx \frac{1}{\Delta t}\frac{1}{\Delta x}\int_{-\Delta x/2}^{\Delta x/2}\int_0^{\Delta t} (-\rho\partial_x\varphi)_{\mathcal{R}}\left(\frac{x}{t}; W_L, W_R\right) dtdx, \\ S^E &\approx \frac{1}{\Delta t}\frac{1}{\Delta x}\int_{-\Delta x/2}^{\Delta x/2}\int_0^{\Delta t} (-q\partial_x\varphi)_{\mathcal{R}}\left(\frac{x}{t}; W_L, W_R\right) dtdx, \end{aligned} \tag{3.10}$$

where S^q and S^E have to be consistent with $-\rho\partial_x\varphi$ and $-q\partial_x\varphi$, in a sense that will be prescribed later. Then, applying the relations from (3.10) to the consistency condition (3.6) results in the following consistency relations, that must be satisfied by the intermediate states:

$$\begin{cases} \rho_L^* + \rho_R^* = 2\rho_{\text{HLL}}, \\ q_L^* + q_R^* = 2q_{\text{HLL}} + \dfrac{S^q\Delta x}{\lambda}, \\ E_L^* + E_R^* = 2E_{\text{HLL}} + \dfrac{S^E\Delta x}{\lambda}. \end{cases} \tag{3.11}$$

In [9] a notation in terms of $\widehat{W}$ and δW given by

$$\widehat{W} = \frac{W_L^* + W_R^*}{2} \qquad \text{and} \qquad \delta W = \frac{W_R^* - W_L^*}{2} \tag{3.12}$$

was introduced, which turned out to be convenient in the derivation of the intermediate states. Therefore, we adopt the same notation and write $W_L^* = \widehat{W} - \delta W$ and $W_R^* = \widehat{W} + \delta W$, with

$$\begin{cases} \widehat{\rho} = \rho_{\text{HLL}}, \\ \widehat{q} = q_{\text{HLL}} + \dfrac{S^q\Delta x}{2\lambda}, \\ \widehat{E} = E_{\text{HLL}} + \dfrac{S^E\Delta x}{2\lambda}. \end{cases} \tag{3.13}$$

In [9] it was shown that the resulting A-RS in terms of (3.13) is consistent. The goal is thus to derive the remaining five unknowns (namely, $\delta\rho$, δq, δE, S^q and S^E) while ensuring positivity, entropy stability and well-balancedness. These notions are precisely defined in Section 3.4, but before that, the next section explains how to use the A-RS (3.2) to perform a time update of the approximation (3.1).

3.3. The Godunov-type finite volume scheme

The intermediate states W_L^* and W_R^* for a first-order scheme are expressed as functions of the left and right states W_L and W_R, as well as the corresponding left and right gravitational potentials φ_L and φ_R. Given that the structure of the A-RS in (3.2) includes a stationary wave with velocity 0, the scheme, as described in [37], is formulated as follows:

$$W_i^{n+1} = W_i^n - \lambda \frac{\Delta t}{\Delta x} \Big[W_L^* \left(W_i^n, W_{i+1}^n, \varphi_i, \varphi_{i+1} \right) - W_R^* \left(W_{i-1}^n, W_i^n, \varphi_{i-1}, \varphi_i \right) \Big]. \tag{3.14}$$

We highlight that the standard conservation form

$$W_i^{n+1} = W_i^n - \frac{\Delta t}{\Delta x} \left(\mathcal{F}(W_i^n, W_{i+1}^n) - \mathcal{F}(W_{i-1}^n, W_i^n) \right) + \frac{\Delta t}{2} \left(\mathcal{S}_{i-\frac{1}{2}}^n + \mathcal{S}_{i+\frac{1}{2}}^n \right), \tag{3.15}$$

is also equivalent to the scheme (3.14). In (3.15), $\mathcal{F}(W_i^n, W_{i+1}^n)$ is the numerical flux and $\mathcal{S}_{i+1/2}^n$ is the numerical source term at interface $x_{i+1/2}$, whose expressions are obtained with straightforward computations presented in e.g. [28]. Setting

$$W_{i+1/2,L}^* = W_L^*(W_{i-1}^n, W_i^n, \varphi_{i-1}, \varphi_i) \quad \text{and} \quad W_{i+1/2,R}^* = W_R^*(W_{i-1}^n, W_i^n, \varphi_{i-1}, \varphi_i), \tag{3.16}$$

we obtain

$$\mathcal{F}(W_i^n, W_{i+1}^n) = \frac{F(W_i^n) + F(W_{i+1}^n)}{2} - \frac{\lambda_{i+\frac{1}{2}}}{2} \left(W_{i+\frac{1}{2},L}^* - W_i^n \right) + \frac{\lambda_{i+\frac{1}{2}}}{2} \left(W_{i+\frac{1}{2},R}^* - W_{i+1}^n \right).$$

The numerical source term is given by

$$\mathcal{S}_{i+\frac{1}{2}}^n = \begin{pmatrix} 0 \\ (S^q)_{i+\frac{1}{2}}^n \\ (S^E)_{i+\frac{1}{2}}^n \end{pmatrix},$$

where $(S^q)_{i+1/2}^n$ and $(S^E)_{i+1/2}^n$ are the source term approximations (3.10) evaluated at the interface $x_{i+\frac{1}{2}}$. Note that if the A-RS fulfills the consistency conditions stated in the previous section, the Godunov-type finite volume scheme (3.15), or (3.14), is consistent. The next section presents other properties that the scheme should satisfy.

3.4. Definitions and conditions to be satisfied by the A-RS

The goal of this section is to present key definitions and provide theoretical results concerning the well-balanced property, positivity, and entropy stability. These concepts are essential for deriving the unknowns in the A-RS, which will be addressed in Sections 3.5 and 3.6. For more details on their motivation, see [9].

3.4.1. Well-balancedness

Recall that we are interested in developing a so-called *fully well-balanced* scheme, which exactly preserves the (moving) steady solutions described in Section 2.1. These solutions are characterized by a constant momentum q, entropy $s(W)$, and specific total enthalpy $H(W, \varphi)$, given by (2.4). This characterization is summarized in the following definition.

Definition 3.1 (Interface Steady Solution (ISS))**.** A pair (W_L, W_R) of admissible states is said to be an Interface Steady Solution (ISS) if, and only if,

$$q_L = q_R, \quad H(W_L, \varphi_L) = H(W_R, \varphi_R), \quad \text{and} \quad s(W_L) = s(W_R).$$

This definition of ISS, allows us to properly define the well-balancedness property.

Definition 3.2 (Well-balancedness)**.** Scheme (3.14) is said to be well-balanced if

$$\forall i \in \mathbb{Z},\ (W_i^n, W_{i+1}^n) \text{ is an ISS} \qquad \Longrightarrow \qquad \forall i \in \mathbb{Z},\ W_i^{n+1} = W_i^n.$$

The following results regarding the connection between ISS and intermediate states were proven in [9].

Lemma 3.3. *Let (W_L, W_R) be an ISS. A sufficient condition for well-balancedness is that $W_L^* = W_L$ and $W_R^* = W_R$.*

Lemma 3.4. *Let (W_L, W_R) be an ISS. Sufficient conditions for well-balancedness are*

$$\widehat{W} = \frac{W_L + W_R}{2} \quad \text{and} \quad \delta W = \frac{W_R - W_L}{2}, \tag{3.17}$$

i.e.,

$$q^* := q_L^* = q_R^*, \qquad H(W_L^*, \varphi_L) = H(W_R^*, \varphi_R), \qquad s^* := s(W_L^*) = s(W_R^*). \tag{3.18}$$

Conditions (3.17) and (3.18) will be crucial in determining the expressions for δW and S^q, S^E in Sections 3.5 and 3.6, respectively.

3.4.2. Entropy stability

The second key property that we wish to satisfy is entropy stability in regions where a convex entropy and associated entropy-entropy flux pair satisfying (2.17) and (2.18) exist. Thus, the following results are presented under this prerequisite.

Definition 3.5 (Entropy stability)**.** The scheme (3.14) is said to be entropy-stable if;, for a convex entropy s, for all smooth functions η satisfying (2.17) and (2.18), and for all $i \in \mathbb{Z}$, the states W_i^n and W_i^{n+1} fulfil the discrete entropy inequality

$$\rho_i^{n+1}\eta(s_i^{n+1}) \leq \rho_i^n \eta(s_i^n) - \frac{\Delta t}{\Delta x}\left((\rho\eta(s)u)_{i+1/2}^n - (\rho\eta(s)u)_{i-1/2}^n\right). \tag{3.19}$$

The following results proven in [9] will be fundamental to reach this important stability property. They rely on the well-known integral entropy consistency, stated in [28].

Lemma 3.6. *If the A-RS given by $\widetilde{W}$ in the form (3.2) satisfies the discrete entropy inequality*

$$\rho_{HLL}\eta(s^*) \leq \big(\rho\eta(s)\big)_{HLL}, \tag{3.20}$$

with ρ_{HLL} defined by (3.7) and $\big(\rho\eta(s)\big)_{HLL}$ defined by (3.9), then the scheme (3.14) is entropy-preserving.

Theorem 3.7 (Theorem 3.5 from [9])**.** *Let $W_L \in \Omega$ and $W_R \in \Omega$ be two given states, let $(\rho s)_{HLL}$ and $\big(\rho\eta(s)\big)_{HLL}$ be defined by (3.8) and (3.9). We adopt a definition of λ such that $\rho_{HLL} > 0$. Then, for all convex smooth functions η, we have*

$$\eta\left(\frac{(\rho s)_{HLL}}{\rho_{HLL}}\right) \leq \frac{\big(\rho\eta(s)\big)_{HLL}}{\rho_{HLL}}. \tag{3.21}$$

Corollary 3.8. *Let*

$$s^* = \frac{(\rho s)_{HLL}}{\rho_{HLL}}. \tag{3.22}$$

Then the integral entropy consistency condition (3.20) is satisfied.

3.4.3. Positivity preservation

The final property we want to preserve is the positivity of the thermodynamic variables, here in terms of density and pressure. The positive of e.g. temperature and internal energy follows immediately from the positivity of the former.

Definition 3.9 (Positivity preservation)**.** Let $W_i^n \in \Omega$ for all $i \in \mathbb{Z}$ and $n \geq 0$. The scheme (3.14) is said to be positivity-preserving if, for all $i \in \mathbb{Z}$, $W_i^{n+1} \in \Omega$, where Ω is the set of admissible states defined in (2.5).

The following result, proven in [9], concerns the positivity of the density. It also holds in the case of a general EOS.

Lemma 3.10 (Density positivity)**.** *Let $W_L \in \Omega$ and $W_R \in \Omega$ two given states. We adopt a definition of λ such that $\rho_{HLL} > 0$. Then,*

$$|\delta\rho| < \rho_{HLL} \tag{3.23}$$

is a sufficient condition for $\rho_L^* > 0$ and $\rho_R^* > 0$.

The positivity of the pressure is closely related to the entropy stability. Thus, the following is a conditional result based on the existence of a convex entropy since it makes use of Theorem 3.7.

Lemma 3.11 (Pressure positivity)**.** *Let $W_L \in \Omega$ and $W_R \in \Omega$ two given states. Let $\rho_L^* > 0$ and $\rho_R^* > 0$, and consider s^* given by (3.22). We adopt a definition of λ such that $\rho_{HLL} > 0$. Then, for all $i \in \mathbb{Z}$, $p_i^{n+1} > 0$.*

3.5. Determination of δW

The objective of this section is to utilize the definitions and conditions introduced in Section 3.4 to derive an expression for the three unknown components of δW, such that $\delta W = [W]/2$ whenever (W_L, W_R) represents an ISS. Here, we denote the jump of a quantity X as $[X] \coloneqq X_R - X_L$. Additionally, for stability reasons, we aim to recover the HLL solver in the absence of a gravitational source term. Thus, we also impose the condition that if $\varphi_L = \varphi_R$, then δW must vanish.

We start with the momentum component δq, Its expression directly derives from (3.18), which states that q_L^* should be equal to q_R^*. Therefore, $\delta q = 0$ is a suitable choice.

Now, we turn to the density component $\delta\rho$. To that end, we will use the ISS property on the specific total enthalpy. Indeed, recall that $H(W_L, \varphi_L) = H(W_R, \varphi_R)$ as soon as (W_L, W_R) is an ISS. Expanding the specific total enthalpy according to its definition (2.4), we obtain a relation on the specific enthalpy h:

$$\frac{E_L + p_L}{\rho_L} + \varphi_L = \frac{E_R + p_R}{\rho_R} + \varphi_R \quad \iff \quad [\varphi] = -[h].$$

Starting from this, the derivation of the expression of $\delta\rho$ is independent of the considered EOS. Namely, it relies on two conditions:

$$[\varphi] = -[h] \implies \delta\rho = \frac{[\rho]}{2} \qquad \text{and} \qquad [\varphi] = 0 \implies \delta\rho = 0.$$

The first one is nothing but the well-balancedness requirement, and the second one corresponds to recovering the HLL solver in the absence of a gravitational source term. However, these conditions are fundamentally incompatible when $[\varphi] = [h] = 0$. Therefore, we relax the second one, to make sure that the scheme remains well-balanced in all situations.

In [9], a formula for $\delta\rho$ was derived for an ideal gas EOS. However, the above-mentioned relaxation relied on taking a limit to be well-defined when $[h]$ vanishes. Here, we derive a new, better-defined expression. It is based on the following lemma, introducing a function ψ and its properties.

Lemma 3.12. *Let ψ be the function defined by*

$$\psi(x, y, \alpha) = \psi_1\big(\psi_2(x, y)\big)^\alpha,$$

where ψ_1 is defined by

$$\psi_1(z) = \cos\left(\frac{\pi}{2}z\right)\exp\left(-2z^2\right),$$

and where ψ_2 is defined by

$$\psi_2(x, y) = \frac{x + y}{\mathcal{M}(\varepsilon_0, \sqrt{x^2 + y^2})}. \tag{3.24}$$

In (3.24), ε_0 is set to 10^{-12}, and $\mathcal{M}$ is a regularized maximum function defined by

$$\mathcal{M}(\varepsilon, z) = \begin{cases} \varepsilon & \text{if } z < \dfrac{\varepsilon}{2}, \\ z & \text{if } z > \dfrac{3\varepsilon}{2}, \\ P(\varepsilon, z) & \text{otherwise,} \end{cases}$$

where P is a polynomial defined such that $\mathcal{M}(\varepsilon_0, \cdot) \in \mathcal{C}^2(\mathbb{R}_+^*, \mathbb{R}_+^*)$:

$$P(\varepsilon, z) = \frac{-z^4}{2\varepsilon^3} + \frac{2z^3}{\varepsilon^2} - \frac{9z^2}{4\varepsilon} + z + \frac{27\varepsilon}{32}.$$

Then, for all $\alpha \in \mathbb{N}$ and $x, y \in \mathbb{R}^2$, ψ satisfies the following properties:

$$\psi(x, y, \alpha) = 1 \iff x = -y, \tag{ψ-i}$$
$$y \geq 3\,\varepsilon_0/2 \implies \psi(0, y, \alpha) = 0, \tag{ψ-ii}$$
$$x \geq 3\,\varepsilon_0/2 \implies \psi(x, 0, \alpha) = 0, \tag{ψ-iii}$$
$$|\psi(x, y, \alpha)| \leq 1, \tag{ψ-iv}$$
$$\psi(\cdot, \cdot, \alpha) \in \mathcal{C}^2(\mathbb{R} \times \mathbb{R}, \mathbb{R}), \tag{ψ-v}$$
$$y \geq 3\,\varepsilon_0/2 \implies \psi(x, y, \alpha) \underset{x \to 0}{=} \mathcal{O}(x^\alpha). \tag{ψ-vi}$$

Proof. The properties (ψ-i)–(ψ-iv) are straightforward, and come from the properties of ψ_1 (proven in [9]). A sketch of ψ is provided in Figure 2 to help the reader understand the function.

To prove (ψ-v), we rely on the values of P and its derivatives:

$$P\left(\varepsilon, \frac{\varepsilon}{2}\right) = \frac{\varepsilon}{2}, \qquad P\left(\varepsilon, \frac{3\varepsilon}{2}\right) = \frac{3\varepsilon}{2},$$
$$\frac{\partial P}{\partial z}\left(\varepsilon, \frac{\varepsilon}{2}\right) = 0, \qquad \frac{\partial P}{\partial z}\left(\varepsilon, \frac{3\varepsilon}{2}\right) = 1,$$
$$\frac{\partial^2 P}{\partial z^2}\left(\varepsilon, \frac{\varepsilon}{2}\right) = 0, \qquad \frac{\partial^2 P}{\partial z^2}\left(\varepsilon, \frac{3\varepsilon}{2}\right) = 0.$$

Therefore, $\mathcal{M}$ is a $\mathcal{C}^2$ function, and so is ψ_2. Since ψ_1 is smooth, ψ turns out to be $\mathcal{C}^2$.

Finally, to prove (ψ-vi), assume that $y \geq 3\,\varepsilon_0/2$. Therefore, for all $x \in \mathbb{R}$,

$$\mathcal{M}(\varepsilon_0, \sqrt{x^2 + y^2}) = \sqrt{x^2 + y^2} = |y| + \mathcal{O}(x^2).$$

Hence,

$$\psi(x,y,\alpha) = \psi_1\left(\frac{x+y}{|y|+\mathcal{O}(x^2)}\right)^{\alpha} = \psi_1\left(\operatorname{sgn}(y)+\mathcal{O}(x)\right)^{\alpha}.$$

However, recall from [9] that $\psi_1(\pm 1 + x) = \mathcal{O}(x)$ as $x \to 0$. Therefore, we have proven that $\psi(x,y,\alpha) = \mathcal{O}(x^{\alpha})$ as $x \to 0$, which concludes the proof. □

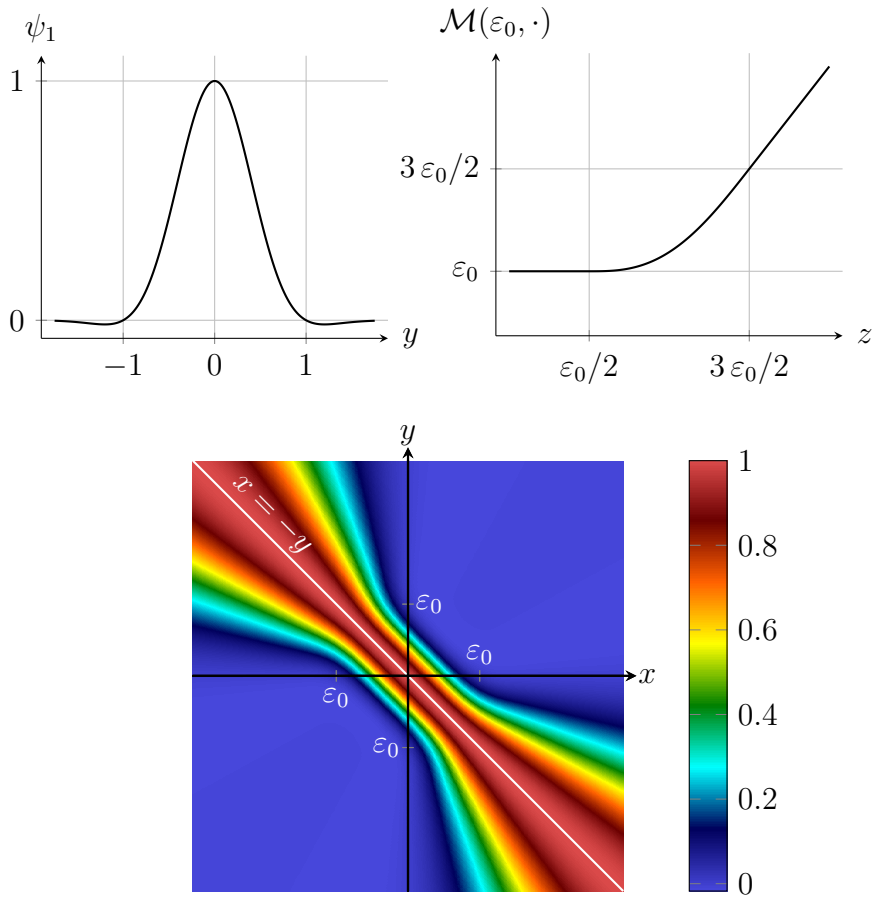

Figure 2: Drawings of the functions ψ_1 (top left panel), $\mathcal{M}$ (top right panel), and ψ (bottom panel).

Equipped with ψ, we are now able to state the expression of $\delta\rho$.

Lemma 3.13. *Let $W_L \in \Omega$ and $W_R \in \Omega$ two given states, and let W_{HLL} be given by (3.7) with sufficiently large λ. Further, let $\delta\rho$ be defined by*

$$\delta\rho = \frac{[\rho]}{2}\,\psi\big([\varphi],[h],1\big).$$

Then, $\delta\rho$ satisfies the following properties:

$$[\varphi] = -[h] \implies \delta\rho = [\rho]/2, \tag{i}$$

$$([\varphi] = 0 \quad \text{and} \quad [h] \geq 3\,\varepsilon_0/2) \implies \delta\rho = 0, \tag{ii}$$

$$([h] = 0 \quad \text{and} \quad [\varphi] \geq 3\,\varepsilon_0/2) \implies \delta\rho = 0, \tag{iii}$$

$$|\delta\rho| \leq \rho_{HLL}. \tag{iv}$$

Proof. Properties (i)–(iv) are straightforward to prove. Indeed, they are directly related to the properties (ψ-i)–(ψ-iv) of ψ, proven in Lemma 3.12. □

Remark 3.14. Property (i) corresponds to the ISS case, and ensures that $\delta\rho$ satisfies (3.17). Property (ii) corresponds to the no-gravity case, and proves that $\delta\rho$ vanishes, leading to $\rho_L^* = \rho_R^* = \rho_{\text{HLL}}$. Property (iii) ensures that $\delta\rho$ is well-defined and vanishes 0 when $[h]$ vanishes. This property involved a limit in [9], whereas the new expression allows it to be directly satisfied. Note that, appropriately, both properties (ii) and (iii) have been relaxed when both $[\varphi]$ and $[h]$ vanish, by introducing ε_0. Property (iv) is the required condition (3.23) from Lemma 3.13 for positivity of the density.

The remaining component δE depends on the EOS, and thus it will be different from the one derived in [9] in the case of the ideal gas law. We use the last remaining ISS condition on s to determine δE. Namely, we impose that, as soon as (W_L, W_R) is an ISS, the entropies of the intermediate states satisfy $s(W_L^*) = s(W_R^*) = s^*$, as prescribed in (3.18). Moreover, due to Corollary 3.8 we know that setting s^* according to (3.22) yields the entropy stability under the prerequisite that a convex entropy exists. Following the discussion from Section 2.2, the expression of the internal energy e with respect to density ρ and entropy s is available. This allows us to define the intermediate internal energies as

$$e_L^* = e(\rho_L^*, s^*), \quad e_R^* = e(\rho_R^*, s^*).$$

Transforming back to the total energy, we obtain, using (2.3),

$$E_L^* = \rho_L^* e_L^* + \frac{q_L^*}{2\rho_L^*} = \widehat{E} - \delta E, \qquad E_R^* = \rho_R^* e_R^* + \frac{q_R^*}{2\rho_R^*} = \widehat{E} + \delta E. \tag{3.25}$$

Since the momentum is constant for an ISS, we replace q_L^* and q_R^* in the above expression with a parameter $\widetilde{q^2}$. Equation (3.25) is nothing but a linear system in $(\widetilde{q^2}, \delta E)$, whose solution is

$$\widetilde{q^2} = \frac{2\rho_L^*\rho_R^*}{\rho_L^* + \rho_R^*}\left(2\widehat{E} - \rho_L^* e_L^* - \rho_R^* e_R^*\right), \qquad \delta E = \frac{1}{2}\left(\rho_R^* e_R^* - \rho_L^* e_L^*\right) + \frac{\widetilde{q^2}}{2}\frac{\delta\rho}{2\rho_L^*\rho_R^*}.$$

Since the derivation started by considering a constant entropy, the above expressions are well-balanced by construction, for any EOS. Moreover, note that the expressions of $\widetilde{q^2}$ and δE derived here are a generalization of the ideal gas case considered in [9], and the above formulas reduce to the ideal gas case when setting $e = (\gamma - 1)\, p/\rho$.

3.6. Determination of S^q and S^E

With the expression for δW established, we now focus on determining the remaining two unknowns, S^q and S^E. To do so, we make use of the expressions for $\widehat{W}$ given in (3.13). Additionally, we recall that if (W_L, W_R) is an ISS, then $\widehat{W} = \overline{W}$, where $\overline{X} \coloneqq (X_L + X_R)/2$ represents the arithmetic mean of the two quantities X_L and X_R. Substituting the expression of W_{HLL} into (3.13), we find that S^q and S^E must satisfy the following conditions when (W_L, W_R) is an ISS:

$$S^q \Delta x = \left(\frac{q_R^2}{\rho_R} + p_R\right) - \left(\frac{q_L^2}{\rho_L} + p_L\right), \tag{3.26a}$$

$$S^E \Delta x = \left(\frac{q_R}{\rho_R}(E_R + p_R)\right) - \left(\frac{q_L}{\rho_L}(E_L + p_L)\right). \tag{3.26b}$$

The goal of this section is to find consistent approximations S^q and S^E of the source term averages satisfying (3.26).

Remark 3.15. Since φ is assumed to be a smooth function, the following holds at each interface:

$$\varphi_R = \varphi_L + \mathcal{O}(\Delta x), \quad \text{i.e.,} \quad [\varphi] = \mathcal{O}(\Delta x).$$

The expression of the energy source term S^E does not depend on the EOS, and thus we directly use the one from [9], summarized in the following lemma.

Lemma 3.16. *Let two given states $W_L \in \Omega$ and $W_R \in \Omega$. Further, let*

$$S^E = -\frac{q_L + q_R}{2} \frac{\varphi_R - \varphi_L}{\Delta x}. \tag{3.27}$$

Then S^E is consistent with $-q\partial_x\varphi$ and satisfies the well-balanced condition (3.26b).

Next, we derive an approximation S^q of the momentum source term such that the ISS condition (3.26a) is satisfied. We make the intuitive Ansatz

$$S^q \Delta x = -\frac{2\rho_L\rho_R}{\rho_L + \rho_R} [\varphi] + \varepsilon, \tag{3.28}$$

where ε accounts for the fact that the first term does not fulfil (3.26a), and therefore a correction, denoted by ε, is needed. We assume that (W_L, W_R) is an ISS. Therefore, in this case,

$$[\varphi] = -\left[e + \frac{p}{\rho} + \frac{1}{2}\frac{q^2}{\rho^2}\right]. \tag{3.29}$$

Equating the right-hand sides of (3.28) and (3.26a), and plugging (3.29), a lengthy but straightforward calculation yields

$$\varepsilon = -\frac{2\rho_L\rho_R}{\rho_L + \rho_R}\left(e(\rho_R, \bar{s}) - e(\rho_L, \bar{s}) + \frac{p(\rho_L, s_L) + p(\rho_R, s_R)}{2}\left(\frac{1}{\rho_R} - \frac{1}{\rho_L}\right)\right). \tag{3.30}$$

As defined above, $\bar{s}$ denotes the arithmetic mean of the left and right entropies. Since ε is not directly consistent with 0 within a shock wave, we proceed as in [9] and multiply it with the function ψ from Lemma 3.12. We summarize the final expression of S^q, and some of its properties, in the following lemma.

Lemma 3.17. *Let two given states $W_L \in \Omega$ and $W_R \in \Omega$. Further, let S^q be given by*

$$S^q = -\frac{2\rho_L\rho_R}{\rho_L + \rho_R}\frac{[\varphi]}{\Delta x} + \frac{\varepsilon}{\Delta x}\,\psi\big([\varphi], [h], 3\big), \tag{3.31}$$

with ε given by (3.30) Then S^q is consistent with $-\rho\partial_x\varphi$ and satisfies the well-balanced condition (3.26a).

Proof. The well-balanced property is satisfied by construction, since $\psi = 1$ as soon as $[\varphi] = -[h]$. It is left to show the consistency. In particular, note that the first term in (3.28) is consistent with $-\rho\partial_x\varphi$ as it is a first order discretization of the source term. Therefore, we need to show that

$$\lim_{\Delta x \to 0} \frac{\varepsilon}{\Delta x}\,\psi\big([\varphi], [h], 3\big) = 0. \tag{3.32}$$

We need to distinguish two cases: (a) the solution is smooth, and (b) the solution is not smooth. In both cases, Remark 3.15 holds, and φ is a smooth function.

(a) We consider a smooth solution, i.e., ρ and s are smooth functions of x. We define the left and right densities as

$$\rho_L = \rho(x), \quad \rho_R = \rho(x + \Delta x).$$

Analogously, we define the left and right entropies. Then, Taylor series expansions yield

$$\frac{e(\rho_R, \bar{s}) - e(\rho_L, \bar{s})}{\Delta x} = \frac{\partial e}{\partial \rho}(\rho(x), \bar{s})\, \partial_x \rho(x) + \mathcal{O}(\Delta x)$$

and

$$\frac{1}{\Delta x}\left[\frac{1}{\rho}\right] = -\frac{\partial_x \rho(x)}{\rho(x)^2} + \mathcal{O}(\Delta x).$$

Using

$$\frac{2\rho_L \rho_R}{\rho_L + \rho_R} = \rho(x) + \mathcal{O}(\Delta x), \quad \frac{p(\rho_L, s_L) + p(\rho_R, s_R)}{2} = p(x) + \mathcal{O}(\Delta x),$$

we obtain

$$\frac{\varepsilon}{\Delta x} = -\rho\, \partial_x \rho \left(\frac{\partial e}{\partial \rho} - \frac{p}{\rho^2}\right) + \mathcal{O}(\Delta x). \tag{3.33}$$

Now, recall from Gibbs' relation that

$$\left(\frac{\partial e}{\partial \rho}\right)_s = \frac{p}{\rho^2},$$

where the subscript s denotes the derivative at constant entropy. Since e is evaluated at the constant entropy $\bar{s}$, (3.33) leads to $\varepsilon/\Delta x = \mathcal{O}(\Delta x)$. Actually, it turns out that the second-order term in the Taylor expansion also vanishes, and we get $\varepsilon/\Delta x = \mathcal{O}(\Delta x^2)$.

(b) Let us now turn to the case where the solution is not smooth, i.e., $W_R = W_L + \mathcal{O}(1)$. In this case, we have $\varepsilon = \mathcal{O}(1)$, and ($\psi$-vi) ensures that $\psi\big([\varphi], [h], 3\big) = \mathcal{O}([\varphi]^3)$. Since φ is smooth, we have $[\varphi] = \mathcal{O}(\Delta x)$, and so $\varepsilon/\Delta x = \mathcal{O}(\Delta x^2)$.

Therefore, in both cases, $\varepsilon/\Delta x = \mathcal{O}(\Delta x^2)$. This means that the consistency requirement (3.32) is satisfied in both cases, which concludes the proof. □

3.7. Summary of the numerical scheme and main properties

We summarize the approximate Riemann solver and state the main properties of the associated Godunov-type finite volume scheme. The A-RS (3.2) is given by

$$\widetilde{W}\left(\frac{x}{t}; W_L, W_R\right) = \begin{cases} W_L & \text{if } x < -\lambda t, \\ W_L^* = \widehat{W} - \delta W & \text{if } -\lambda t < x < 0, \\ W_R^* = \widehat{W} + \delta W & \text{if } 0 < x < \lambda t, \\ W_R & \text{if } x > \lambda t, \end{cases} \tag{3.34}$$

where the components of $\widehat{W}$ are given by

$$\begin{cases} \widehat{\rho} = \rho_{\text{HLL}}, \\ \widehat{q} = q_{\text{HLL}} + \dfrac{S^q \Delta x}{2\lambda}, \\ \widehat{E} = E_{\text{HLL}} + \dfrac{S^E \Delta x}{2\lambda}, \end{cases} \tag{3.35}$$

with W_{HLL} given by (3.7) and the approximate wave speed λ satisfying (3.4). In (3.35), the source term approximations S^q and S^E are respectively given by (3.31) and (3.27), i.e.,

$$\begin{aligned} S^q &= -\frac{2\rho_L\rho_R}{\rho_L+\rho_R}\frac{\varphi_R-\varphi_L}{\Delta x} + \frac{\varepsilon}{\Delta x}\,\psi\big(\varphi_R-\varphi_L, h_R-h_L, 3\big), \\ S^E &= -\frac{q_L+q_R}{2}\frac{\varphi_R-\varphi_L}{\Delta x}, \end{aligned} \tag{3.36}$$

where ψ is defined in Lemma 3.12, and where ε satisfies, according to (3.30),

$$\varepsilon = -\frac{2\rho_L\rho_R}{\rho_L+\rho_R}\left(e(\rho_R,\bar{s}) - e(\rho_L,\bar{s}) + \frac{p(\rho_L,s_L)+p(\rho_R,s_R)}{2}\left(\frac{1}{\rho_R}-\frac{1}{\rho_L}\right)\right),$$

with $\bar{s} = (s_L+s_R)/2$. To define δW, we need the intermediate quantities

$$s^* = \frac{(\rho s)_{\mathrm{HLL}}}{\rho_{\mathrm{HLL}}}, \qquad e_L^* = e(\rho_L^*, s^*) \qquad \text{and} \qquad e_R^* = e(\rho_R^*, s^*).$$

The components of δW are then constructed in Section 3.5, and they satisfy

$$\begin{cases} \delta\rho = \dfrac{\rho_R-\rho_L}{2}\,\psi\big(\varphi_R-\varphi_L, h_R-h_L, 1\big), \\ \delta q = 0, \\ \delta E = \dfrac{1}{2}\left(\rho_R^* e_R^* - \rho_L^* e_L^*\right) + \dfrac{1}{4}\dfrac{\rho_R^*-\rho_L^*}{\rho_L^*+\rho_R^*}\left(2\widehat{E} - \rho_L^* e_L^* - \rho_R^* e_R^*\right). \end{cases} \tag{3.37}$$

The properties of the numerical scheme are summarized in the main result.

Theorem 3.18. *Let the time step Δt be given by (3.5) and assume that the initial data satisfies $W_i^0 \in \Omega$ for all $i \in \mathbb{Z}$. Then, the numerical scheme (3.14) with the approximate Riemann solver (3.34), where $\widehat{W}$ is given by (3.35) and δW is given by (3.37), satisfies the following properties:*

1. *consistency with the Euler system (2.1);*
2. *positivity of the density: for all $n \geq 0$,*

$$\forall i \in \mathbb{Z},\ \rho_i^n > 0 \quad \Longrightarrow \quad \forall i \in \mathbb{Z},\ \rho_i^{n+1} > 0;$$

further, if system (2.1) is equipped with a convex entropy satisfying the entropy inequality (2.17) for all smooth functions η satisfying (2.18), then the stronger result holds: for all $n \geq 0$,

$$\forall i \in \mathbb{Z},\ W_i^n \in \Omega \quad \Longrightarrow \quad \forall i \in \mathbb{Z},\ W_i^{n+1} \in \Omega;$$

3. *entropy stability: if system (2.1) is equipped with a convex entropy satisfying the entropy inequality (2.17) for all smooth functions η satisfying (2.18), then for all $i \in \mathbb{Z}$, for all $n \geq 0$ holds*

$$\rho_i^{n+1}\eta(s_i^{n+1}) \leq \rho_i^n\eta(s_i^n) - \frac{\Delta t}{\Delta x}\left((\rho\eta(s)u)_{i+1/2}^n - (\rho\eta(s)u)_{i-1/2}^n\right);$$

4. *well-balancedness:*

$$\forall i \in \mathbb{Z},\ (W_i^n, W_{i+1}^n) \text{ is an ISS} \quad \Longrightarrow \quad \forall i \in \mathbb{Z},\ W_i^{n+1} = W_i^n.$$

Proof. We prove the four properties in order, using the results derived in the previous sections.

1. According to [28], the scheme is consistent as soon as the A-RS satisfies the integral consistency relation, see Section 3.2. The A-RS has been constructed such that this relation holds, and thus it is consistent. Therefore, the numerical scheme (3.14) is also consistent.

2. The positivity of the density is guaranteed by that of the intermediate densities. Indeed, according to Lemma 3.13, the intermediate densities satisfy the positivity condition (3.23). Therefore, $\rho_L^* > 0$ and $\rho_R^* > 0$ in the A-RS, and thus $\rho_i^{n+1} > 0$ in the numerical scheme. Further, if system (2.1) is equipped with an entropy inequality, then Lemma 3.11 can also be applied, yielding the positivity of the pressure $p_i^{n+1} > 0$.

3. Assuming that the system is endowed with an entropy inequality, the entropy stability of the scheme is ensured as soon as the intermediate entropy satisfies the entropy inequality (3.20). Corollary 3.8 gives an expression for this intermediate entropy, which is used to build the A-RS (3.34). This proves that the scheme is entropy-stable.

4. Lemma 3.3 gives a sufficient condition for well-balancedness, which leads to the conditions (3.17) on $\widehat{W}$ and δW used in (3.34) to define the A-RS. Sections 3.5 and 3.6 constructs $\widehat{W}$ and δW such that the conditions (3.17) are satisfied, and consequently the numerical scheme is well-balanced.

All four properties have been proven, and the proof is thus concluded. □

4. Numerical results

In this section, we perform numerical test cases to validate the theoretical properties of the first-order well-balanced scheme described in Theorem 3.18. In addition, we provide a well-balanced high-order extension of this scheme, based on the systematic technique outlined in [6] and used in e.g. [38, 8] for the shallow water equations and [9] for the Euler system. This technique relies on the fact that, for steady solutions, the well-balanced scheme is exact while the high-order scheme is not. Hence, we compute the distance between the current solution and a steady solution by checking the error in the ISS condition Definition 3.1 at each interface. This allows us to define an indicator, relying on a parameter C_θ to be determined for each test case, that detects whether the current solution is steady, and uses the first-order scheme accordingly. In general, decreasing the value of C_θ leads to a higher sensitivity with respect to the equilibrium state. This results in a high-order well-balanced scheme that does not require solving any non-linear system of equations. The first, second and third order fully well-balanced schemes are respectively denoted by FWB1, FWB2 and FWB3. The FWB2 scheme is constructed with the minmod limiter in the reconstruction, see for instance [51], and uses the SSP-RK2 time integrator, while the FWB3 scheme makes uses the third order TVD reconstruction from [43] and the SSP-RK3 time integrator. Both Runge-Kutta schemes are standard schemes that can be found for instance in [26].

In all test cases, we apply six different EOSs to assess the performance of the numerical schemes. Four applied EOS are obtained from the cubic EOS (2.13), namely the ideal gas law (denoted by `ideal`), the van-der-Waals gas (denoted by `vdW`), the Redlich-Kwong EOS (denoted by `R-K`), and the Peng-Robinson EOS (denoted by `P-R`). The free parameters of these four cubic EOSs are given in Table 3. The remaining two EOSs are tabulated and are obtained by using the `CoolProp` library [2]. The first tabulated EOS, denoted by $\texttt{H}_2\texttt{O}$, models the properties of water, while the second one, denoted by $\texttt{CH}_4$, includes the physical properties of methane.

	ideal	vdW	R-K	P-R
$R\,[\mathrm{J\,K^{-1}}]$	0.4	0.4	0.4	0.4
$c_v^0\,[\mathrm{J\,K^{-1}}]$	1	1	1	1
$s_0\,[\mathrm{J\,K^{-1}}]$	$\log(0.4)$	$\log(0.4)$	0	0
$a_0\,[^{(a)}]$	—	$15.67^{(b)}$	15	15
$b\,[\mathrm{m^3\,kg^{-1}}]$	—	$0.1273^{(b)}$	0.05	0.05
$T_0\,[\mathrm{K}]$	—	—	—	0.3
κ	—	—	—	0.5

Table 3: Parameters for the ideal gas, van-der-Waals, Redlich-Kwong and Peng-Robinson EOS. A dash indicates that the parameter is not used. Notes: (a) the unit of a_0 is $\mathrm{m^6K^{1/2}/kg^2}$ for `R-K` and $\mathrm{m^6/kg^2}$ for the other three EOSs; (b) the values of a_0 and b for the van-der-Waals EOS are modified in Section 4.3.1.

Further, if not otherwise specified, we apply in all test cases the quadratic gravitational potential

$$\varphi(x) = \frac{\varphi_0}{2}(x - x_0)^2. \tag{4.1}$$

The scaling factor φ_0 ensures that the flow is within the same Mach and Froude number regime. Therefore, φ_0 depends on the typical magnitude of the equilibrium pressure and density. We set $\varphi_0 = 2 \cdot 10^4\,\mathrm{s^{-2}}$ for both tabulated EOSs due to the physical properties of water and methane at normal pressure, i.e. Mach numbers around 10^{-2}, and $\varphi_0 = 1\,\mathrm{s^{-2}}$ for the four analytical EOSs which corresponds to Mach regimes around 1. For more details on well-balanced methods for low Mach and Froude number regimes and formal Mach and Froude number limits for the Euler equations with gravity, see e.g. [47].

Unless otherwise mentioned, the parameter Λ in the eigenvalue estimate (3.4) is set to 1. The same applies to the parameter C_θ which in the high-order scheme is in general set to 1 for the `ideal`, $\mathtt{H_2O}$ and $\mathtt{CH_4}$ EOSs, and set to 5 for the `vdW`, `R-K` and `P-R` EOSs.

4.1. Accuracy of the numerical schemes

To verify the experimental order of convergence (EOC) of the numerical schemes, we study an exact solution for the Euler equations with gravity (2.1) taken from [32], which is a variation of the test introduced in [56]. The analytical solution, with constant velocity u_0, is given by

$$\begin{cases} \rho(x,t) = \rho_0 \left(1 + A \sin\left(k\pi(x - u_0 t)\right)\right), \\ u(x,t) = u_0, \\ p(x,t) = p_0 - \rho_0 \left((x - u_0 t) - \dfrac{A}{k\pi} \cos\left(k\pi(x - u_0 t)\right)\right). \end{cases} \tag{4.2}$$

We take $k = 4$, which yields a highly oscillatory solution. The other parameters are given in Table 4 with respect to each used EOS. Indeed, since all EOSs have different domains of validity, the parameters differ for each EOS. This test case is designed for a linear potential $\varphi(x) = x$. The simulation is carried out on the computational domain $\Omega = [0, 1]$, on seven grids with $N = 16 \cdot 2^j$ cells, where $j \in \{0, \dots, 6\}$ with exact boundary conditions. The final time if $t_\mathrm{f} = 10^{-5}\,\mathrm{s}$ for both tabulated EOSs, and $t_\mathrm{f} = 0.5\,\mathrm{s}$ for the other four EOSs.

In Figure 3, the L^2 errors are depicted with respect to the number of discretization cells. We recover the expected EOC for all schemes independently of the considered EOS.

	ideal	vdW	R-K	P-R	H_2O	CH_4
ρ_0 [kg m^{-3}]	2	2	2	10	997.05	422.8
u_0 [m s^{-1}]	0.25	0.25	0.25	0.25	1250	1000
p_0 [Pa]	5	20	5	15	101 800	101 800
A	0.25	0.1	0.25	0.025	10^{-4}	10^{-3}

Table 4: Parameters of the exact solution (4.2) from Section 4.1, for each of the six EOSs under consideration.

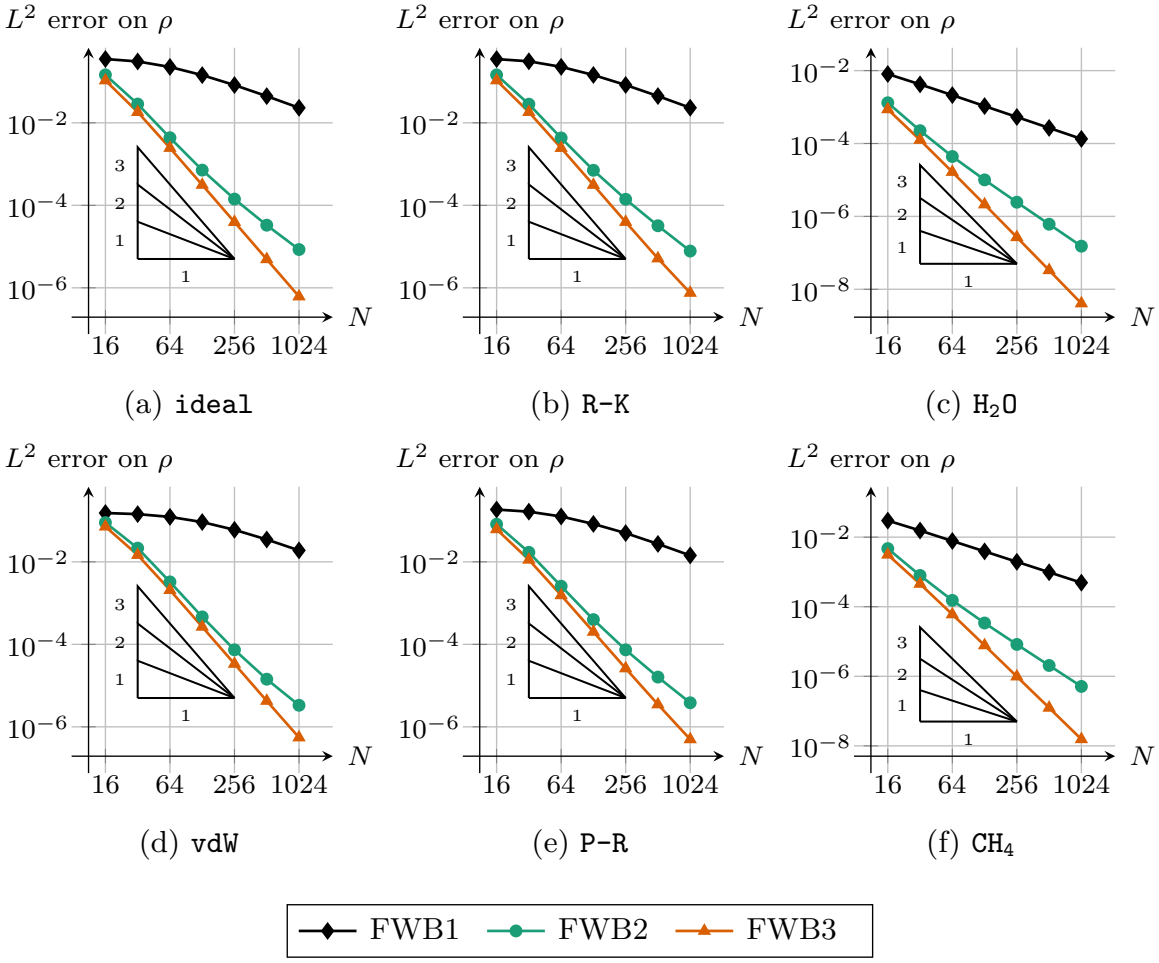

Figure 3: Experimental order of convergence and L^2 errors between the exact solution (4.2) and its approximation by the schemes FWB1, FWB2 and FWB3, for each of the six EOSs under consideration.

4.2. Assessment of the well-balanced property

The main motivation behind the construction of well-balanced schemes in general lies in the resolution of small perturbations around equilibria using coarse meshes. Applying a non-well-balanced scheme on those computational conditions easily leads to huge background errors stemming from the low resolution of the equilibrium state which makes the numerical solution unusable. Thus, capturing in particular delicate perturbations would require a substantial grid refinement to reduce the truncation error and make the perturbations visible.

The next three sets of test cases therefore concern the performance of the novel fully well-balanced solvers on such flows on coarse grids. The first one validates the exact preservation of a moving steady

solution, whereas the subsequent two are dedicated to studying perturbations of such equilibria.

The equilibrium solution is computed from the triplet (q_0, s_0, H_0) given, with respect to each EOS, in Table 5. In all cases, the computational domain is $\Omega = [0, 1]$ and the gravitational potential is given by (4.1). The final times, for each experiment, are reported in Table 6 which differ for each EOS due to different flow regimes inflicted by initial condition and EOS.

EOS	$q_0 \left[\frac{\text{kg}}{\text{m}^2\,\text{s}}\right]$	$s_0 \left[\frac{\text{J}}{\text{K}}\right]$	$H_0 \left[\frac{\text{m}^2}{\text{s}^2}\right]$
`ideal`	1	1	5
`vdW`	2.5	-3.0	55.0
`R-K`	1	-2.5	12.5
`P-R`	5	-2	20
`H2O`	10^5	$6.7 \cdot 10^2$	$2.1 \cdot 10^5$
`CH4`	10^5	-80	$2.5 \cdot 10^4$

Table 5: Values of the constant discharge q_0, entropy s_0 and specific total enthalpy H_0 for the moving equilibrium test cases from Section 4.2.

EOS	t_f [s], Section 4.2.1	t_f [s], Section 4.2.2	t_f [s], Section 4.2.3
`ideal`	1.5	0.05	0.72
`vdW`	1.5	0.02	0.72
`R-K`	1.5	0.05	0.72
`P-R`	0.1	0.01	1.34
`H2O`	10^{-4}	10^{-4}	$7.2 \cdot 10^{-4}$
`CH4`	$2 \cdot 10^{-3}$	10^{-4}	$7.2 \cdot 10^{-4}$

Table 6: Values of the final time t_f for the moving equilibrium test cases from Section 4.2.

4.2.1. Preservation of a moving steady solution

To numerically verify the well-balanced property of the schemes, we first compute the time evolution of the equilibrium solution with nonzero velocity. We take 50 discretization cells, and apply exact boundary conditions. We expect the solution to remain exact, up to machine precision, when using our fully well-balanced scheme. To avoid scaling issues, we take $C_\theta = 10^{-4}$ for the `H2O` EOS and $C_\theta = 2 \cdot 10^{-3}$ for the `CH4` EOS.

The L^2 errors at time $t = t_\text{f}$ are given in Table 7. All well-balanced schemes are able to preserve the moving equilibrium up to machine precision for all considered EOS, whereas the classical HLL scheme [28] yields quite large errors. This verifies and illustrates the ability of the new well-balanced solvers to capture moving equilibria up to machine precision for general EOS.

4.2.2. Gaussian perturbation of a moving steady solution

Next, we consider a Gaussian perturbation of a moving equilibrium. This is a standard test case whose purpose is to verify that underlying equilibrium does not inflict spurious errors in the perturbation. The computational domain is discretized using 50 cells, with inhomogeneous Dirichlet boundary

		HLL	FWB1	FWB2	FWB3
ideal	ρ	$3.94 \cdot 10^{-3}$	$2.30 \cdot 10^{-15}$	$2.72 \cdot 10^{-15}$	$2.53 \cdot 10^{-15}$
	q	$3.38 \cdot 10^{-5}$	$1.03 \cdot 10^{-16}$	$1.23 \cdot 10^{-16}$	$1.50 \cdot 10^{-16}$
	E	$3.38 \cdot 10^{-5}$	$1.03 \cdot 10^{-16}$	$1.23 \cdot 10^{-16}$	$1.50 \cdot 10^{-16}$
vdW	ρ	$3.97 \cdot 10^{-5}$	$7.02 \cdot 10^{-16}$	$4.08 \cdot 10^{-16}$	$4.56 \cdot 10^{-16}$
	q	$6.29 \cdot 10^{-7}$	$4.40 \cdot 10^{-17}$	$4.86 \cdot 10^{-17}$	$4.40 \cdot 10^{-17}$
	E	$2.18 \cdot 10^{-6}$	$1.74 \cdot 10^{-16}$	$2.80 \cdot 10^{-16}$	$3.69 \cdot 10^{-16}$
R-K	ρ	$2.15 \cdot 10^{-4}$	$2.19 \cdot 10^{-15}$	$1.18 \cdot 10^{-15}$	$9.37 \cdot 10^{-16}$
	q	$8.76 \cdot 10^{-6}$	$9.79 \cdot 10^{-17}$	$8.25 \cdot 10^{-17}$	$9.39 \cdot 10^{-17}$
	E	$2.87 \cdot 10^{-5}$	$3.44 \cdot 10^{-16}$	$3.01 \cdot 10^{-16}$	$3.82 \cdot 10^{-16}$
P-R	ρ	$9.83 \cdot 10^{-5}$	$1.95 \cdot 10^{-14}$	$1.64 \cdot 10^{-14}$	$1.64 \cdot 10^{-14}$
	q	$4.40 \cdot 10^{-5}$	$3.83 \cdot 10^{-15}$	$2.06 \cdot 10^{-15}$	$3.34 \cdot 10^{-15}$
	E	$2.68 \cdot 10^{-5}$	$1.14 \cdot 10^{-14}$	$1.12 \cdot 10^{-14}$	$1.02 \cdot 10^{-14}$
H_2O	ρ	$1.13 \cdot 10^{-5}$	$5.52 \cdot 10^{-14}$	$4.02 \cdot 10^{-14}$	$3.94 \cdot 10^{-14}$
	q	$8.07 \cdot 10^{-7}$	$4.67 \cdot 10^{-14}$	$1.71 \cdot 10^{-13}$	$1.64 \cdot 10^{-13}$
	E	$1.16 \cdot 10^{-5}$	$1.09 \cdot 10^{-13}$	$2.51 \cdot 10^{-13}$	$2.26 \cdot 10^{-13}$
CH_4	ρ	$5.40 \cdot 10^{-6}$	$1.46 \cdot 10^{-15}$	$9.88 \cdot 10^{-16}$	$8.41 \cdot 10^{-16}$
	q	$5.11 \cdot 10^{-5}$	$1.70 \cdot 10^{-13}$	$1.85 \cdot 10^{-13}$	$1.86 \cdot 10^{-13}$
	E	$1.13 \cdot 10^{-4}$	$4.68 \cdot 10^{-14}$	$4.21 \cdot 10^{-14}$	$5.19 \cdot 10^{-14}$

Table 7: Well-balanced test case from Section 4.2: L^2 errors on the density, the momentum and the total energy, reported for each of the six EOSs.

conditions corresponding to the exact, unperturbed steady solution. From the triplet (q_0, s_0, H_0) reported in Table 5, we compute the equilibrium state $(\rho_{\text{eq}}, u_{\text{eq}}, p_{\text{eq}})$. Then, the initial density and velocity are set to $\rho(x,0) = \rho_{\text{eq}}(x)$ and $u(x,0) = u_{\text{eq}}$, while a small perturbation is added to the pressure, i.e.,

$$p(x,0) = p_{\text{eq}}(x)\left(1 + \nu \exp\left(-100\left(x - \frac{1}{2}\right)^2\right)\right).$$

The parameter ν denotes the amplitude of the initial perturbation, and is set to $\nu = 10^{-4}$. Different choices of ν yield similar numerical results and are thus omitted. Moreover, we take $C_\theta = 10^{-10}$ for the H_2O EOS and $C_\theta = 10^{-9}$ for the CH_4 EOS, i.e. we increase the sensitivity in detection of the equilibrium states when employing the high order reconstruction.

In Figure 4 we plot the relative density perturbation $\eta_\rho = (\rho_{\text{eq}}(x) - \rho)/\rho_{\text{eq}}$, scaled with respect to the background equilibrium $\rho_{\text{eq}}(x)$, at the final time $t = t_{\text{f}}$. The considered times guarantee that the waves triggered by the perturbation are still contained inside the computational domain. The perturbations for all considered EOS are well-captured and no spurious errors are introduced from the background equilibrium.

4.2.3. Sinusoidal perturbation of a moving steady solution

Another test case of interest consists in a moving steady solution perturbed by a wave created by a time-dependent boundary condition and propagating into the computational domain. Similar set-ups can be found in [22], motivated by the study of wave propagation in stellar atmospheres. Here, we

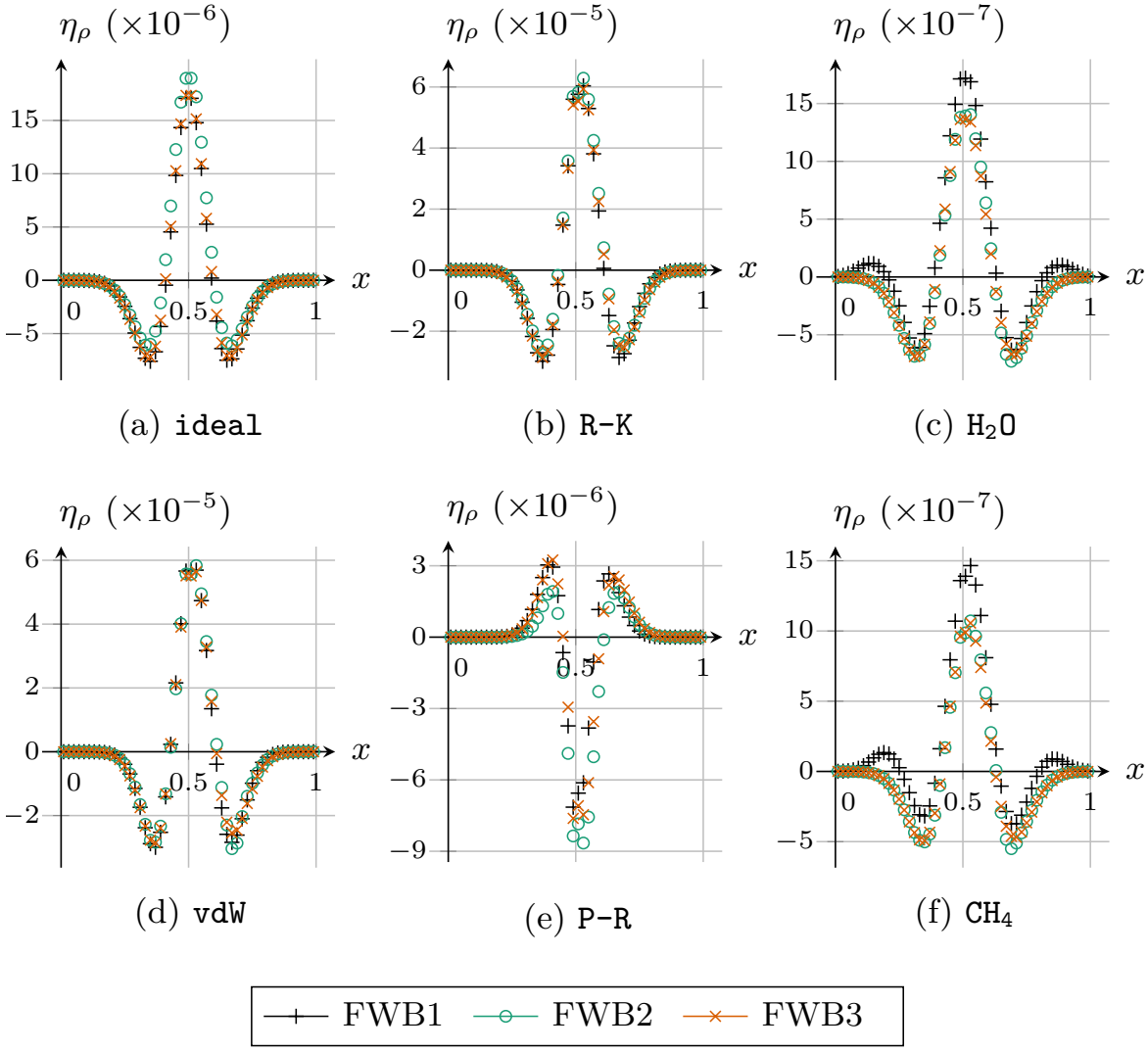

Figure 4: Perturbation of equilibrium state, described in Section 4.2.2: Relative density difference $\eta_\rho = (\rho_{\text{eq}}(x) - \rho)/\rho_{\text{eq}}(x)$ with respect to the equilibrium density $\rho_{\text{eq}}(x)$, where ρ is obtained by the schemes FWB1, FWB2 and FWB3 respectively, using the six EOSs under consideration.

consider the same moving equilibrium as above, described by (q_0, s_0, H_0) in Table 5. The computational domain contains 512 cells. The finer mesh is motivated by the high oscillatory perturbation and visualization purposes. The perturbation is applied onto the momentum as a right (left for P-R) boundary condition. It is given for $t > 0$ by

$$q(x_0, t) = q_0\big(1 + \nu \sin(\kappa\pi t)\big). \tag{4.3}$$

Therein ν denotes the amplitude of the perturbation and κ its frequency and $x_0 \in \{0, 1\}$ corresponds to the excited boundary condition. Moreover, $q_0 > 0$ is the steady momentum reported in Table 5 for each EOS respectively, and so the flow travels from left to right. Based on the same motivation as in the test cases above, these parameters are chosen differently for each EOS and summarized in Table 8. The parameter x_0 is taken equal to 1 to perturb the right boundary, except for the P-R EOS where we take $x_0 = 0$. Indeed, for the P-R EOS, all waves travel towards the right. Therefore, perturbing the left boundary for the P-R EOS allows us to observe the waves propagating through the computational domain. For the other five EOSs, waves travel in both directions, and thus we

perturb the right boundary to observe the waves going upwind wih respect to the flow direction. The simulation is stopped as the perturbation reaches the opposite boundary of the computational domain. Due to the different initial conditions and configurations of the EOSs, the final time t_f differs and are reported in Table 6. In addition, the parameters of the high-order schemes are set to $C_\theta = 10^{-12}$ for the $\mathtt{H_2O}$ and $\mathtt{CH_4}$ EOSs.

EOS	ν	κ [Hz]	Λ
`ideal`	10^{-8}	8	1.5
`vdW`	10^{-8}	16	2.5
`R-K`	10^{-8}	16	1.5
`P-R`	10^{-10}	16	1.5
$\mathtt{H_2O}$	10^{-5}	$16 \cdot 10^3$	1.1
$\mathtt{CH_4}$	$5 \cdot 10^{-6}$	$16 \cdot 10^3$	1.1

Table 8: Steady solution perturbed at the boundary: required values of the parameters. The values of the perturbation constants are reported, alongside the final time and value of the wave speed factor Λ.

The relative difference between numerical results and the moving equilibrium are given in Figure 5. Note that we have modified the factor Λ in the wave speed estimate, to introduce some additional numerical viscosity to stabilize the numerical scheme, see Table 8. These changes are marginally and are necessary since the well-balanced scheme drastically reduces the numerical viscosity by construction.

We observe that the perturbations remain well-resolved for all considered EOS despite being of orders around 10^{-9} in some cases. Note that, for the `P-R` EOS, the pressure perturbation is displayed instead of the velocity perturbation. This is due to the steady state being supercritical, and thus the perturbations in u quickly leave the domain, while the acoustic waves remain visible as pressure perturbations.

4.3. Riemann Problems

As a final series of test cases, we consider three Riemann Problems (RPs), two classical ones for the Euler equations without a source term, and one in presence of a gravitational field, far from an equilibrium.

In all these cases, the space domain is $\Omega = [0, 1]$, and we prescribe homogeneous Neumann boundary conditions. Moreover, the initial condition takes the form of a Riemann problem, i.e.,

$$W(x, 0) = \begin{cases} W_L & \text{if } x < x_0, \\ W_R & \text{if } x \geq x_0, \end{cases}$$

with the jump position $x_0 = 0.5$. The left and right states depend on the problem under consideration. In each case, we take a grid consisting of 75 cells.

4.3.1. Homogeneous case

We first consider RPs without the influence of the gravitational field, i.e. we set $\varphi = 0$. Note that, for the `vdW` EOS, we set $a_0 = 2\,\mathrm{m}^6/\mathrm{kg}^2$ and $b = 0.5\,\mathrm{m}^3\,\mathrm{kg}^{-1}$, to have solutions closer to the `ideal` EOS, and to check the impact of this more complex EOS on classical RPs.

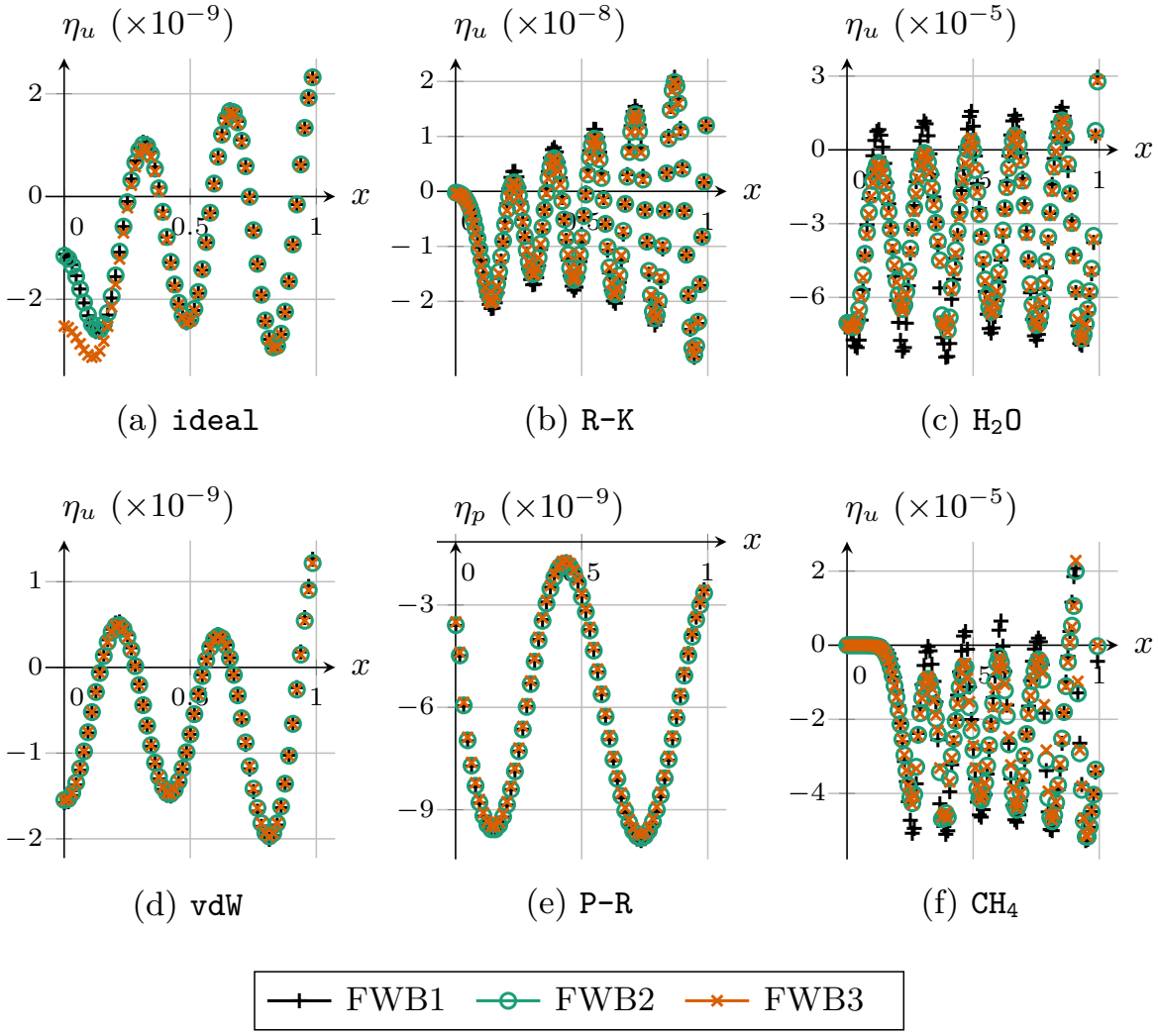

Figure 5: Boundary perturbation of equilibrium state, described in Section 4.2.3: Relative velocity perturbation $\eta_u = (u_{\text{eq}}(x) - u)/u_{\text{eq}}(x)$ or relative pressure perturbation $\eta_p = (p_{\text{eq}}(x) - p)/p_{\text{eq}}(x)$, with respect to the equilibrium velocity $u_{\text{eq}}(x)$ or pressure $p_{\text{eq}}(x)$ respectively, where u or p are obtained by the schemes FWB1, FWB2 and FWB3, using the six EOSs under consideration.

We first consider a set of Sod-like RPs, whose left and right states are given for each EOS in Table 9. The numerical results for ρ, u and p are given in Figures 6 to 8, respectively. We observe that the first order scheme is quite diffusive, in particular on contact and shock waves, throughout all considered EOS. As its order of accuracy increases, the new well-balanced scheme captures each wave more accurately. As is typical for high-order schemes, small oscillations can be observed near the shock waves. However, all schemes are able to correctly determine the shock position and amplitude independently of the applied EOS. The numerical results are compared against a reference solution obtained with the classical HLL scheme [28] using 7500 cells. We observe a good agreement with the reference solution. Note, however, that the contact discontinuity has been quite diffused in the H_2O case (sub-figures (c)). This leads to a perturbation of the plateau in the velocity profile.

We then turn to a double rarefaction, whose initial data for all EOS is given by

$$\rho_L = \rho_R = \rho_0, \quad q_L = -q_0, \quad q_R = q_0, \quad p_L = p_R = p_0. \tag{4.4}$$

The initial data is detailed in Table 10. This is a challenging problem, as it can lead to a near-vacuum

EOS		$\rho\,\left[\frac{\text{kg}}{\text{m}^3}\right]$	$u\,\left[\frac{\text{m}}{\text{s}}\right]$	$p\,[\text{Pa}]$	$t_\text{f}\,[\text{s}]$
`ideal`	L	1	0	1	0.1644
	R	0.125	0	0.1	
`vdW`	L	1	0	1	0.1644
	R	0.125	0	0.1	
`R-K`	L	1.5	0	1.25	0.25
	R	0.5	0	0.75	
`P-R`	L	1.5	0	1.5	0.25
	R	0.35	0	0.15	
$\texttt{H}_2\texttt{O}$	L	996	0	10^6	$2 \cdot 10^{-4}$
	R	998	0	10^5	
$\texttt{CH}_4$	L	422	0	10^7	$2 \cdot 10^{-4}$
	R	424	0	10^5	

Table 9: Initial conditions for the Sod-like Riemann problems. Initial states left (L) and right (R) are reported for density, velocity and pressure as well as the final time t_f.

state in the center of the domain. The results are displayed for the density in Figure 9 at the final times reported in Table 10. A similar behavior is obtained for the pressure. However, due to the similarity in the results, we have omitted the pressure plots. Despite the fact that ρ and p are very close to zero in the center of the domain, see e.g. the `ideal`, `vdW` or $\texttt{CH}_4$ EOS, no negative values of ρ and p are observed nor the simulation had to be stopped. The numerical results for the schemes FWB1, FWB2 and FWB3 are compared against a reference solution obtained with the classical HLL scheme [28] using 7500 cells.

EOS	$\rho_0\,\left[\frac{\text{kg}}{\text{m}^3}\right]$	$q_0\,\left[\frac{\text{kg}}{\text{m}^2\,\text{s}}\right]$	$p_0\,[\text{Pa}]$	$t_\text{f}\,[\text{s}]$
`ideal`	1	10/3	1	0.075
`vdW`	1	10/3	1	0.065
`R-K`	1	1.8	1	0.125
`P-R`	1	1.5	1	0.125
$\texttt{H}_2\texttt{O}$	997.05	59.9	101 325	$1.75 \cdot 10^{-4}$
$\texttt{CH}_4$	0.657	1789	101 325	10^{-4}

Table 10: Initial conditions for the double rarefaction Riemann problems. The initial density, momentum and pressure is reported, as well as the final time t_f, for each EOS.

4.3.2. Riemann problem in a gravitational field

The last Riemann problem is a Sod-like problem in the presence of the quadratic gravitational source term (4.1). The initial data is given in steady variables q, s and H, and is reported in Table 11,

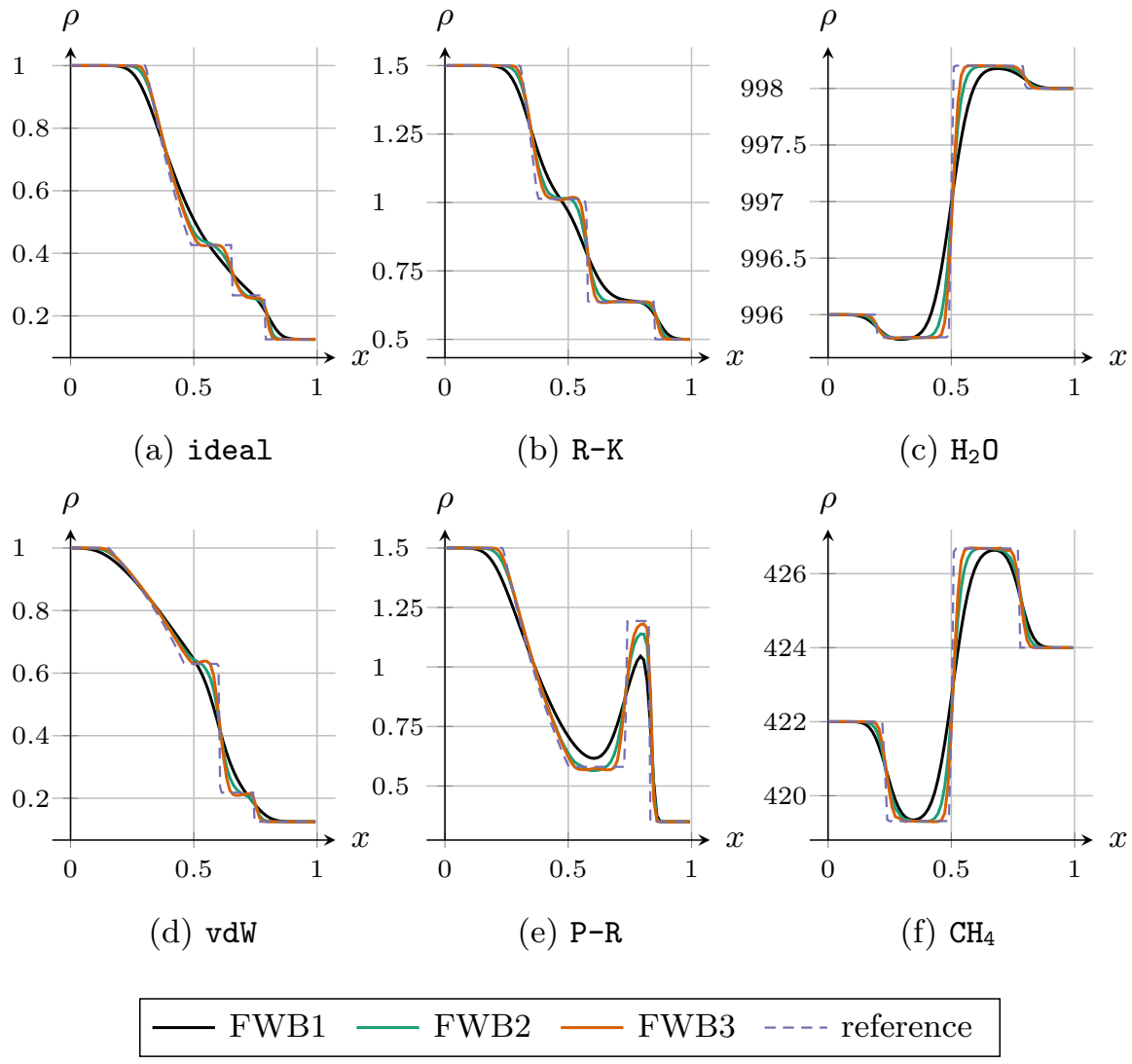

Figure 6: Sod-like Riemann Problems: Density ρ at final time for the schemes FWB1, FWB2 and FWB3 for the six EOSs. For each EOS, the final time, as well as the left and right states, are reported in Table 9.

alongside the final time t_f, for each EOS. Note that, for the P-R EOS, we set the initial jump position to $x_0 = 0.8$, since all waves travel towards the left of the domain. The equilibrium variables are displayed in Figures 10 to 12. We observe that the solution generated by the new well-balanced scheme accurately captures the arising shock and rarefaction waves. The numerical results are compared against a reference solution obtained with the classical HLL scheme with a centered discretization of the source terms on 7500 cells.

5. Conclusions

In this paper, we derived a new numerical scheme to approximate weak solutions of the Euler equations with a gravitational source term with general equations of state which can be given analytically or tabulated. The presented Godunov-type finite volume scheme is based on an approximate Riemann solver composed of two intermediate states. It is constructed such that the scheme is consistent, fully well-balanced and preserves the positivity of the density. Moreover, if the system is equipped with a convex entropy and an associated entropy inequality holds, the scheme is entropy-stable and the

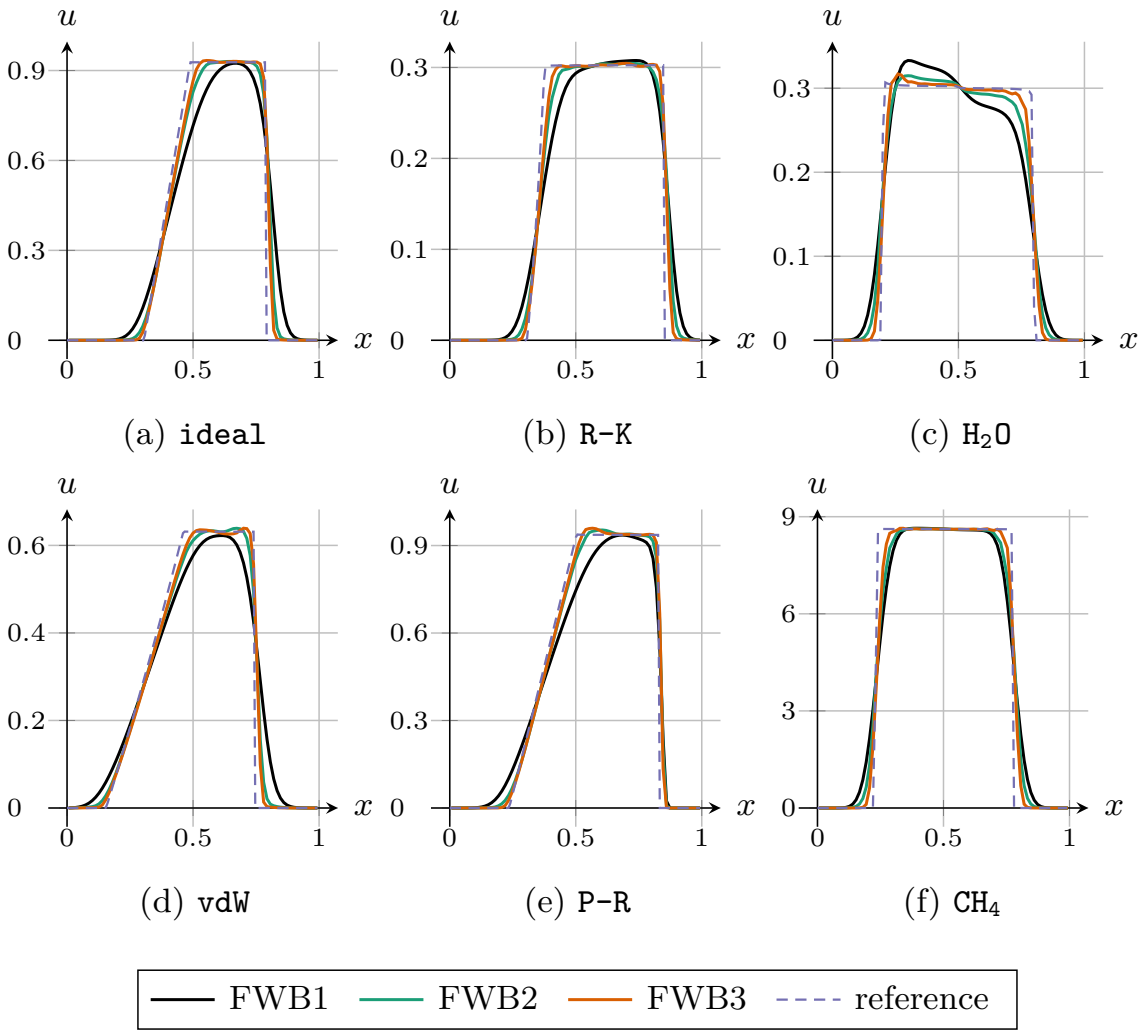

Figure 7: Sod-like Riemann Problems: Velocity u at final time for the schemes FWB1, FWB2 and FWB3 for the six EOSs. For each EOS, the final time, as well as the left and right states, are reported in Table 9.

positivity of thermodynamical variables is ensured. The proof of these properties are summarized in Theorem 3.18. The results presented in this work are an extension of the fully well-balanced scheme for the ideal gas law detailed in Berthon et al. [9]. In this spirit, the scheme coincides with the well-known HLL Riemann solver in the absence of a gravitational field. This first order scheme is then extended to higher order using a well-known strategy in the context of Godunov-type schemes for the shallow water equations [6, 38]. The theoretical findings are validated numerically by computing moving equilibrium solutions as well as the propagation of perturbations and Riemann Problems using three different analytically given equations of states as well as two tabulated equations of state based on the `CoolProp` library [2].

Acknowledgments

V. Michel-Dansac extends his thanks to ANR-22-CE25-0017 OptiTrust. The SHARK-FV conference has greatly contributed to this work.

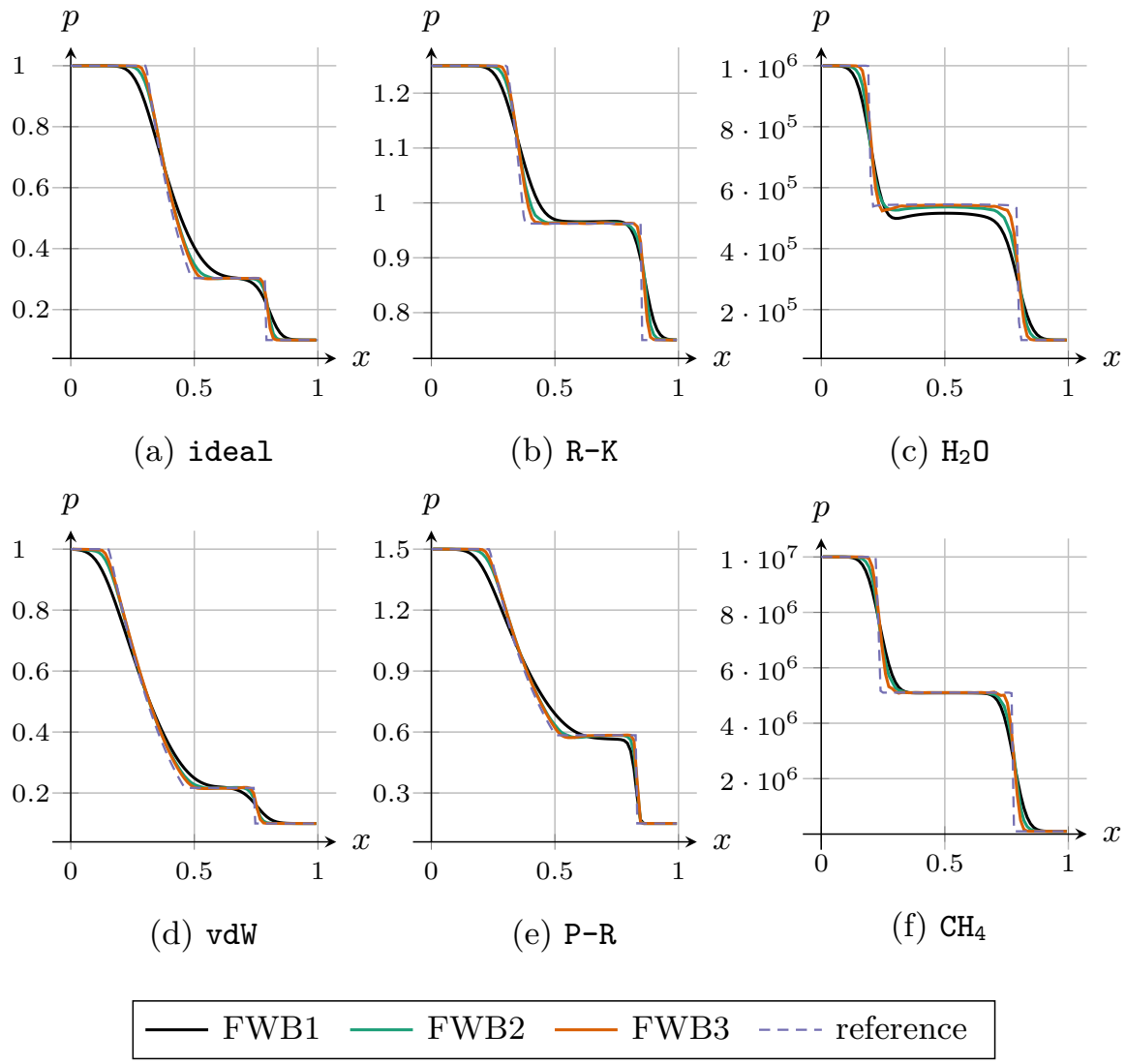

Figure 8: Sod-like Riemann Problems: Pressure p at final time for the schemes FWB1, FWB2 and FWB3 for the six EOSs. For each EOS, the final time, as well as the left and right states, are reported in Table 9.

A. Entropy conditions

To determine conditions on the convexity of a sufficiently smooth mathematical entropy $U(W) = \rho\eta(s)$ for a specific entropy s fulfilling Gibbs' relations (2.2), we consider the sub-determinants of the Hessian matrix $H = \nabla_W^2 U(W)$. Further, we make use of the relations

$$\frac{\partial^2 s}{\partial \tau^2} = -\frac{T\partial_\tau p - p\partial_\tau T}{T^2}, \qquad \frac{\partial^2 s}{\partial e^2} = \frac{\partial_e T}{T^2}, \qquad \frac{\partial^2 s}{\partial \tau \partial e} = \frac{\partial_\tau T}{T^2}.$$

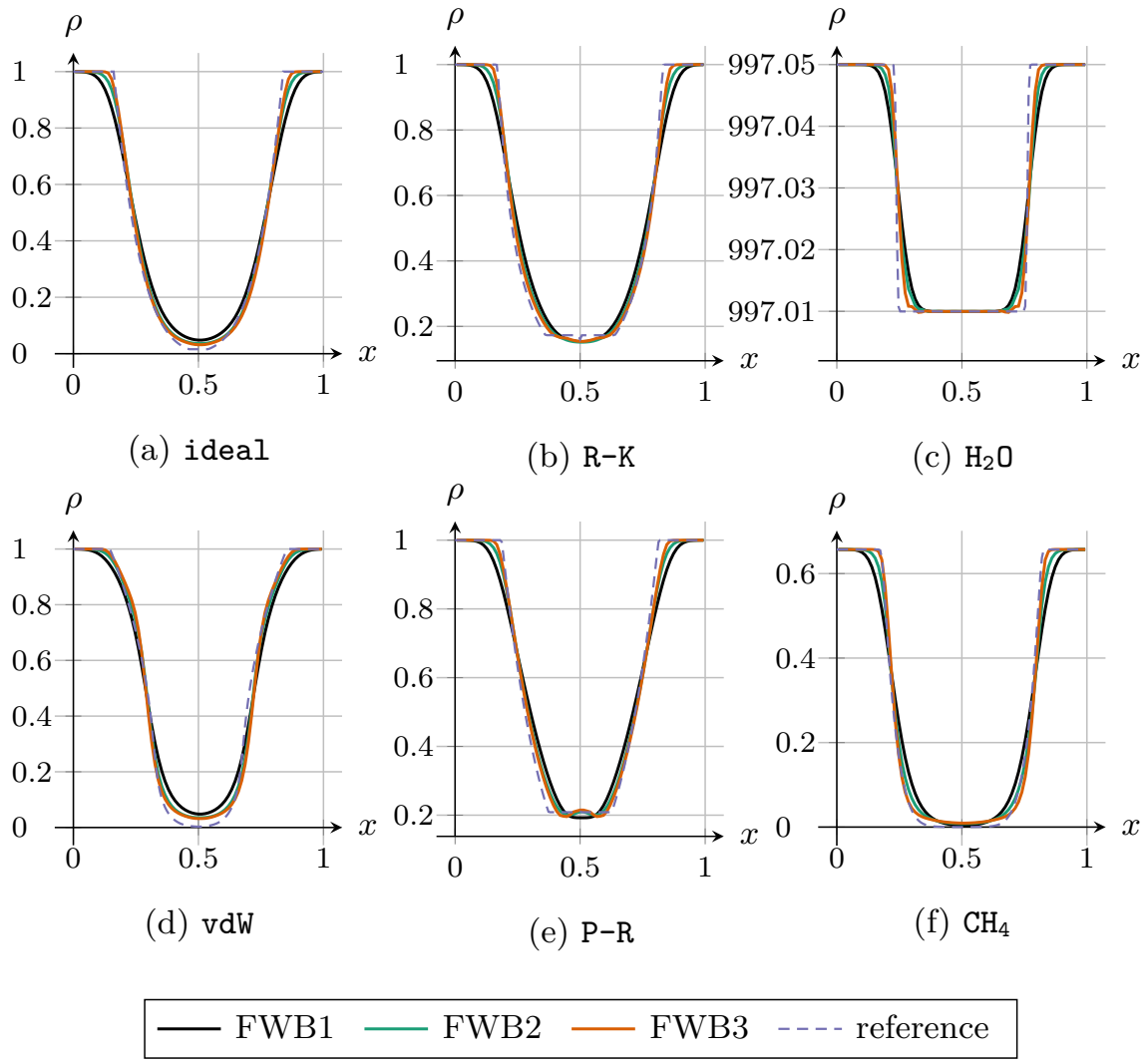

Figure 9: Double rarefaction test case: Density ρ at final time for the schemes FWB1, FWB2 and FWB3 for the six EOSs. For each EOS, the final time, as well as the initial condition, are reported in Table 10.

From the sub-determinants of H, we obtain the three conditions

$$\begin{cases} \big(-(\partial_\tau T)^2 + \partial_e T(p\partial_\tau T - T\partial_\tau p)\big)\eta'(s) \\ \qquad + \big(p^2\partial_e T - p\partial_\tau T - T\partial_\tau p\big)\eta''(s) \geq 0, \\ \Big(\partial_\tau T(2\rho e - \rho u^2) + \partial_e T(\rho e - \frac{1}{2}\rho u^2)^2 + (p\partial_\tau T - T\partial_\tau p) + u^2\rho^2 T\Big)\eta'(s) \\ \qquad\qquad + \Big(p - \frac{1}{2}\rho u^2 + \rho e\Big)^2 \eta''(s) \geq 0, \\ \Big(u^2\Big(-(\partial_\tau T)^2 + \partial_e T(p\partial_\tau T - T\partial_\tau p)\Big) + T\Big(\partial_\tau T(2E+p) + \partial_e T E^2 - T\partial_\tau p\Big)\Big)\eta'(s) \\ \qquad\qquad + \Big(u^2\Big(p^2\partial_e T - p\partial_\tau T - T\partial_\tau p\Big) + T(E+p)^2\Big)\eta''(s) \geq 0. \end{cases}$$

Note that this is only one way to find conditions on the convexity of $U(W)$ and the conditions are sufficient, but not necessarily necessary.

EOS		$q\left[\frac{\text{kg}}{\text{m}^2\,\text{s}}\right]$	$s\left[\frac{\text{J}}{\text{K}}\right]$	$H\,[\text{J}]$	$t_\text{f}\,[\text{s}]$
`ideal`	L	1	0.1	6	0.15
	R	0	0.3	3	
`vdW`	L	1	-3.25	780	0.05
	R	2.5	-3	55	
`R-K`	L	2	-2.75	25	0.09
	R	1	-2.5	12.5	
`P-R`	L	-5	-2	15	0.1
	R	-4	-3	30	
H_2O	L	10^5	$6.7 \cdot 10^2$	$2.1 \cdot 10^5$	$2 \cdot 10^{-3}$
	R	10^4	$1.5 \cdot 10^3$	$5 \cdot 10^5$	
CH_4	L	10^5	-80	$2.5 \cdot 10^4$	$2 \cdot 10^{-3}$
	R	10^4	-20	10^5	

Table 11: Initial conditions for the Sod-like Riemann problems in a gravitational field. Initial states left (L) and right (R) are reported for momentum q, specific entropy s and specific total enthalpy H; the final time t_f is also reported.

References

[1] E. Audusse, F. Bouchut, M.-O. Bristeau, R. Klein, and B. Perthame. A fast and stable well-balanced scheme with hydrostatic reconstruction for shallow water flows. *SIAM J. Sci. Comput.*, 25(6):2050–2065, 2004.

[2] I. H. Bell, J. Wronski, S. Quoilin, and V. Lemort. Pure and pseudo-pure fluid thermophysical property evaluation and the open-source thermophysical property library coolprop. *Ind. Eng. Chem. Res.*, 53(6):2498–2508, 2014.

[3] J. P. Berberich, P. Chandrashekar, and C. Klingenberg. High order well-balanced finite volume methods for multi-dimensional systems of hyperbolic balance laws. *Comput. & Fluids*, 219:104858, 2021.

[4] J. P. Berberich, R. Käppeli, P. Chandrashekar, and C. Klingenberg. High Order Discretely Well-Balanced Methods for Arbitrary Hydrostatic Atmospheres. *Commun. Comput. Phys.*, 30(3):666–708, 2021.

[5] C. Berthon. Numerical approximations of the 10-moment gaussian closure. *Math. Comp.*, 75(256):1809–1832, 2006.

[6] C. Berthon, S. Bulteau, F. Foucher, M. M'Baye, and V. Michel-Dansac. A Very Easy High-Order Well-Balanced Reconstruction for Hyperbolic Systems with Source Terms. *SIAM J. Sci. Comput.*, 44(4):A2506–A2535, 2022.

[7] C. Berthon and F. Foucher. Efficient well-balanced hydrostatic upwind schemes for shallow-water equations. *J. Comput. Phys.*, 231(15):4993–5015, 2012.

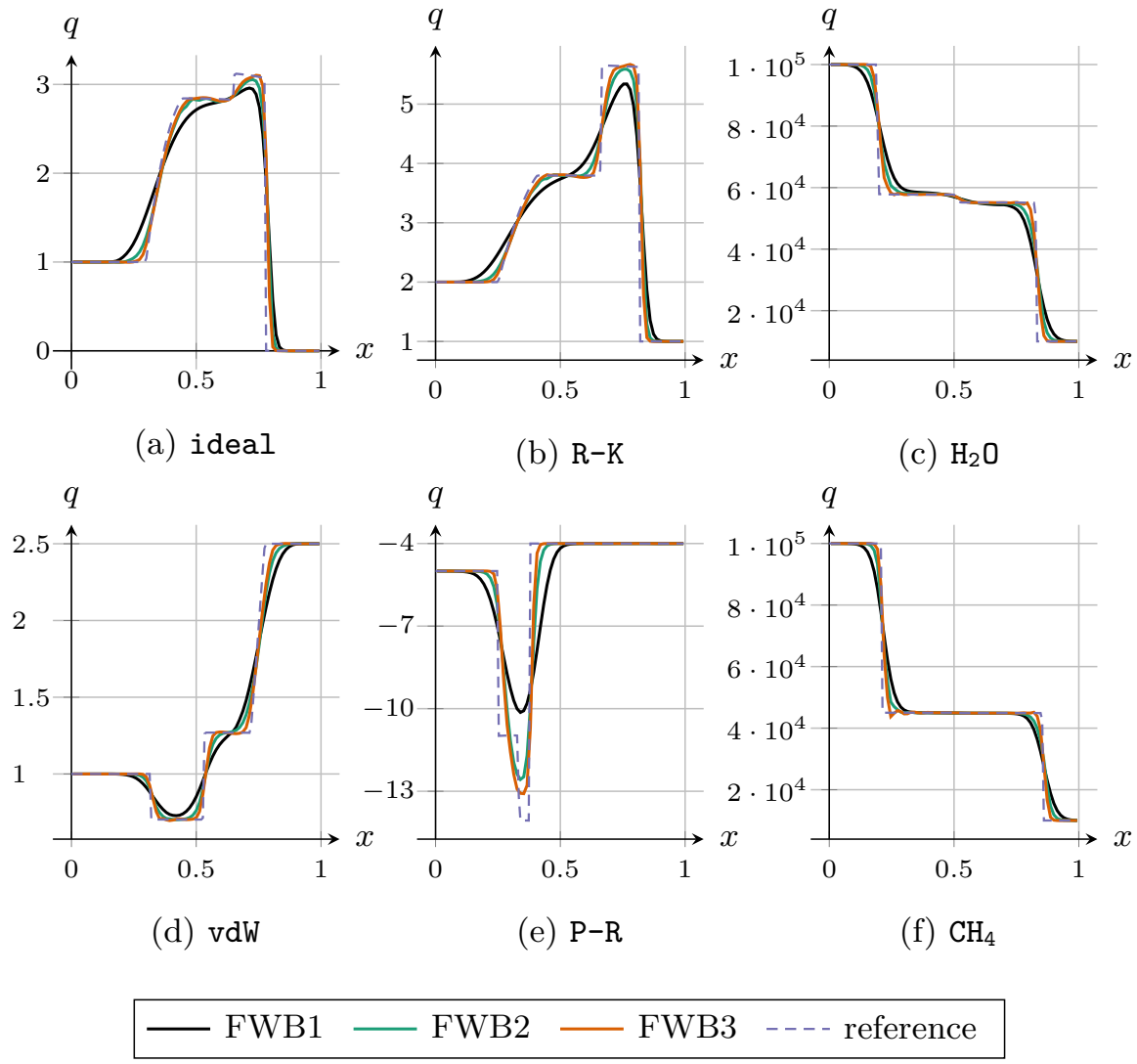

Figure 10: Sod-like Riemann Problems in a gravitational field: Momentum q at final time for the schemes FWB1, FWB2 and FWB3 for the six EOSs. For each EOS, the final time, as well as the left and right states, are reported in Table 11.

[8] C. Berthon and V. Michel-Dansac. A fully well-balanced hydrodynamic reconstruction. *J. Numer. Math.*, 32(3):275–299, 2024.

[9] C. Berthon, V. Michel-Dansac, and A. Thomann. An entropy-stable and fully well-balanced scheme for the Euler equations with gravity. *arXiv, //arxiv.org/pdf/2406.15051v1*, 2024.

[10] F. Bouchut. *Nonlinear stability of finite volume methods for hyperbolic conservation laws and well-balanced schemes for sources*. Frontiers in Mathematics. Birkhäuser Verlag, Basel, 2004.

[11] J. Britton and Y. Xing. High Order Still-Water and Moving-Water Equilibria Preserving Discontinuous Galerkin Methods for the Ripa Model. *J. Sci. Comput.*, 82(2), 2020.

[12] C. Caballero-Cárdenas, M. J. Castro, T. Morales de Luna, and M. L. Muñoz-Ruiz. Implicit and implicit-explicit Lagrange-projection finite volume schemes exactly well-balanced for 1D shallow water system. *Appl. Math. Comput.*, 443:127784, 2023.

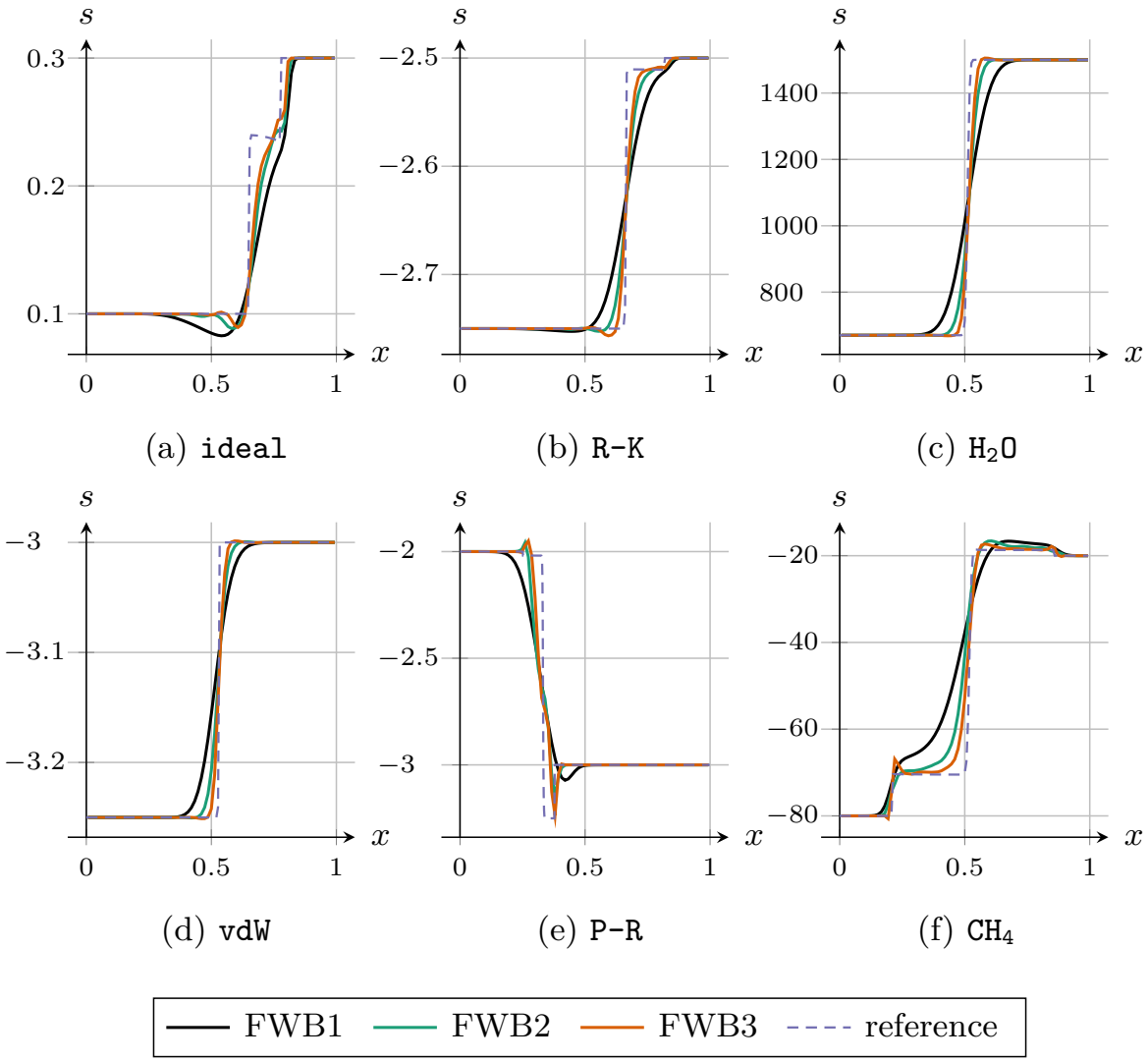

Figure 11: Sod-like Riemann Problems in a gravitational field: Specific entropy s at final time for the schemes FWB1, FWB2 and FWB3 for the six EOSs. For each EOS, the final time, as well as the left and right states, are reported in Table 11.

[13] P. Cargo and A.-Y. Le Roux. Un schéma équilibre adapté au modèle d'atmosphère avec termes de gravité. *C. R. Acad. Sci., Paris, Sér. I*, 318(1):73–76, 1994.

[14] M. Castro, J. M. Gallardo, J. A. López-García, and C. Parés. Well-balanced high order extensions of Godunov's method for semilinear balance laws. *SIAM J. Numer. Anal.*, 46(2):1012–1039, 2008.

[15] M. J. Castro, A. Pardo Milanés, and C. Parés. Well-balanced numerical schemes based on a generalized hydrostatic reconstruction technique. *Math. Models Methods Appl. Sci.*, 17(12):2055–2113, 2007.

[16] M. J. Castro and C. Parés. Well-Balanced High-Order Finite Volume Methods for Systems of Balance Laws. *J. Sci. Comput.*, 82(2), 2020.

[17] C. Chalons and J.-F. Coulombel. Relaxation approximation of the Euler equations. *J. Math. Anal. Appl.*, 348(2):872–893, 2008.

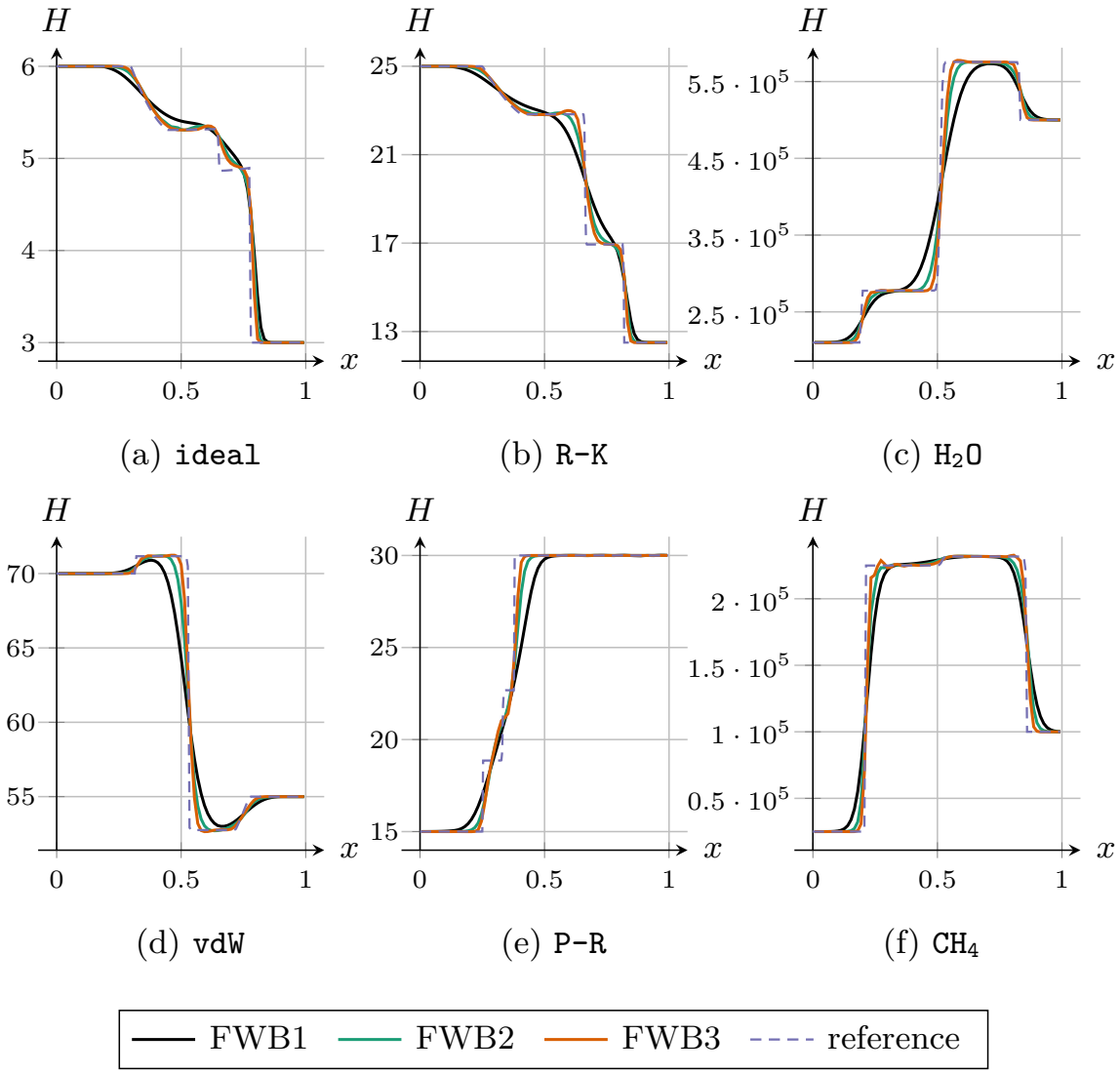

Figure 12: Sod-like Riemann Problems in a gravitational field: Specific total enthalpy H at final time for the schemes FWB1, FWB2 and FWB3 for the six EOSs. For each EOS, the final time, as well as the left and right states, are reported in Table 11.

[18] G. Chen and S. Noelle. A new hydrostatic reconstruction scheme based on subcell reconstructions. *SIAM J. Numer. Anal.*, 55(2):758–784, 2017.

[19] V. Desveaux, M. Zenk, C. Berthon, and C. Klingenberg. A well-balanced scheme to capture non-explicit steady states in the Euler equations with gravity. *Int. J. Numer. Methods Fluids*, 81(2):104–127, 2016.

[20] E. Feireisl, M. Lukáčová-Medviďová, H. Mizerová, and B. She. *Numerical Analysis of Compressible Fluid Flows*. Springer International Publishing, 2021.

[21] E. Franck, V. Michel-Dansac, and L. Navoret. Approximately well-balanced Discontinuous Galerkin methods using bases enriched with Physics-Informed Neural Networks. *J. Comput. Phys.*, 512:113144, 2024.

[22] F. G. Fuchs, A. D. McMurry, S. Mishra, N. H. Risebro, and K. Waagan. High order well-balanced

finite volume schemes for simulating wave propagation in stratified magnetic atmospheres. *J. Comput. Phys.*, 229(11):4033–4058, 2010.

[23] E. Gaburro, M. J. Castro, and M. Dumbser. Well-balanced Arbitrary-Lagrangian-Eulerian finite volume schemes on moving nonconforming meshes for the Euler equations of gas dynamics with gravity. *Mon. Not. R. Astron Soc.*, 477(2):2251–2275, 2018.

[24] E. Godlewski and P.-A. Raviart. *Hyperbolic systems of conservation laws*, volume 3/4 of *Mathématiques & Applications (Paris) [Mathematics and Applications]*. Ellipses, Paris, 1991.

[25] I. Gómez-Bueno, M. J. Castro Díaz, C. Parés, and G. Russo. Collocation Methods for High-Order Well-Balanced Methods for Systems of Balance Laws. *Mathematics*, 9(15):1799, July 2021.

[26] S. Gottlieb, C.-W. Shu, and E. Tadmor. Strong stability-preserving high-order time discretization methods. *SIAM Rev.*, 43(1):89–112, 2001.

[27] L. Grosheintz-Laval and R. Käppeli. Well-balanced finite volume schemes for nearly steady adiabatic flows. *Journal of Computational Physics*, 423:109805, December 2020.

[28] A. Harten, P. D. Lax, and B. van Leer. On upstream differencing and Godunov-type schemes for hyperbolic conservation laws. *SIAM Rev.*, 25(1):35–61, 1983.

[29] P. Helluy and H. Mathis. Pressure laws and fast Legendre transform. *Math. Models Method Appl. Sci.*, 21(04):745–775, 2011.

[30] R. Käppeli and S. Mishra. Well-balanced schemes for the Euler equations with gravitation. *J. Comput. Phys.*, 259:199–219, 2014.

[31] R. Käppeli and S. Mishra. Well-balanced schemes for the Euler equations with gravitation. *J. Comput. Phys.*, 259:199–219, 2014.

[32] C. Klingenberg, G. Puppo, and M. Semplice. Arbitrary Order Finite Volume Well-Balanced Schemes for the Euler Equations with Gravity. *SIAM J. Sci. Comput.*, 41(2):A695–A721, 2019.

[33] R. Käppeli. Well-balanced methods for computational astrophysics. *Living Reviews in Computational Astrophysics*, 8(1), October 2022.

[34] R. J. LeVeque and D. S. Bale. Wave propagation methods for conservation laws with source terms. In Rolf Jeltsch and Michael Fey, editors, *Hyperbolic Problems: Theory, Numerics, Applications*, volume 130 of *International Series of Numerical Mathematics*, pages 609–618. Birkhäuser Basel, 1999.

[35] G. Li and Y. Xing. Well-balanced discontinuous Galerkin methods with hydrostatic reconstruction for the Euler equations with gravitation. *J. Comput. Phys.*, 352:445–462, 2018.

[36] Y. Mantri, P. Öffner, and M. Ricchiuto. Fully well-balanced entropy controlled discontinuous Galerkin spectral element method for shallow water flows: Global flux quadrature and cell entropy correction. *J. Comput. Phys.*, 498:112673, February 2024.

[37] V. Michel-Dansac, C. Berthon, S. Clain, and F. Foucher. A well-balanced scheme for the shallow-water equations with topography. *Comput. Math. Appl.*, 72(3):568–593, 2016.

[38] V. Michel-Dansac, C. Berthon, S. Clain, and F. Foucher. A two-dimensional high-order well-balanced scheme for the shallow water equations with topography and Manning friction. *Comput. & Fluids*, 230:105152, 2021.

[39] S. Noelle, Y. Xing, and C.-W. Shu. High-order well-balanced finite volume WENO schemes for shallow water equation with moving water. *J. Comput. Phys.*, 226(1):29–58, 2007.

[40] C. Parés and M. Castro. On the well-balance property of Roe's method for nonconservative hyperbolic systems. Applications to shallow-water systems. *M2AN Math. Model. Numer. Anal.*, 38(5):821–852, 2004.

[41] D.-Y. Peng and D. B. Robinson. A new two-constant equation of state. *Ind. Eng. Chem., Fundam.*, 15(1):59–64, 1976.

[42] O. Redlich and J. N. S. Kwong. On the thermodynamics of solutions. V. an equation of state. Fugacities of gaseous solutions. *Chem. Rev.*, 44(1):233–244, February 1949.

[43] B. Schmidtmann, B. Seibold, and M. Torrilhon. Relations Between WENO3 and Third-Order Limiting in Finite Volume Methods. *J. Sci. Comput.*, 68(2):624–652, 2015.

[44] U. Setzmann and W. Wagner. A New Equation of State and Tables of Thermodynamic Properties for Methane Covering the Range from the Melting Line to 625 K at Pressures up to 1000 MPa. *J. Phys. Chem. Ref. Data*, 20(6):1061–1155, 1991.

[45] E. Tadmor. A minimum entropy principle in the gas dynamics equations. *Appl. Numer. Math.*, 2(3-5):211–219, 1986.

[46] E. Tadmor. Entropy stability theory for difference approximations of nonlinear conservation laws and related time-dependent problems. *Acta Numer.*, 12:451–512, May 2003.

[47] A. Thomann, G. Puppo, and C. Klingenberg. An all speed second order well-balanced IMEX relaxation scheme for the Euler equations with gravity. *J. Comput. Phys.*, 420:109723, 2020.

[48] A. Thomann, M. Zenk, and C. Klingenberg. A second-order positivity-preserving well-balanced finite volume scheme for Euler equations with gravity for arbitrary hydrostatic equilibria. *Int. J. Numer. Methods Fluids*, 89(11):465–482, 2019.

[49] E. F. Toro. *Riemann solvers and numerical methods for fluid dynamics*. Springer-Verlag, Berlin, third edition, 2009. A practical introduction.

[50] J. D. Van Der Waals. Doctoral dissertation. *Leiden, Holland*, 1873.

[51] B. van Leer. Towards the Ultimate Conservative Difference Scheme, V. A Second Order Sequel to Godunov's Method. *J. Comput. Phys.*, 32:101–136, 1979.

[52] D. Varma and P. Chandrashekar. A second-order, discretely well-balanced finite volume scheme for euler equations with gravity. *Comput. & Fluids*, 281:292–313, March 2019.

[53] J. Vides, B. Braconnier, A. Audit, C. Berthon, and B. Nkonga. A Godunov-type solver for the numerical approximation of gravitational flows. *Comm. Comput. Phys.*, 15:46–75, 2014.

[54] W. Wagner and A. Pruß. The IAPWS Formulation 1995 for the Thermodynamic Properties of Ordinary Water Substance for General and Scientific Use. *J. Phys. Chem. Ref. Data*, 31(2):387–535, 2002.

[55] Y. Xing. Exactly well-balanced discontinuous Galerkin methods for the shallow water equations with moving water equilibrium. *J. Comput. Phys.*, 257(part A):536–553, 2014.

[56] Y. Xing and C.-W. Shu. High Order Well-Balanced WENO Scheme for the Gas Dynamics Equations Under Gravitational Fields. *J. Sci. Comput.*, 54(23):645–662, 2012.

[57] Y. Xing, X. Zhang, and C.-W. Shu. Positivity-preserving high order well-balanced discontinuous Galerkin methods for the shallow water equations. *Adv. Water Resour.*, 33(12):1476–1493, 2010.